



**HAL**  
open science

## Class III peroxidases PRX01, PRX44, and PRX73 potentially target extensins during root hair growth in *Arabidopsis thaliana*

Eliana Marzol, Cecilia Borassi, Mariana Carignani Sardoy, Philippe Ranocha, Ariel A Aptekman, Mauro Bringas, Janice Pennington, Julio Paez-Valencia, Javier Martínez Pacheco, Diana R Rodríguez-García, et al.

### ► To cite this version:

Eliana Marzol, Cecilia Borassi, Mariana Carignani Sardoy, Philippe Ranocha, Ariel A Aptekman, et al.. Class III peroxidases PRX01, PRX44, and PRX73 potentially target extensins during root hair growth in *Arabidopsis thaliana*. *International Journal of Molecular Sciences*, 2022, 23 (10), pp.5375. 10.3390/ijms23105375 . hal-03799581

**HAL Id: hal-03799581**

**<https://hal.science/hal-03799581>**

Submitted on 6 Oct 2022

**HAL** is a multi-disciplinary open access archive for the deposit and dissemination of scientific research documents, whether they are published or not. The documents may come from teaching and research institutions in France or abroad, or from public or private research centers.

L'archive ouverte pluridisciplinaire **HAL**, est destinée au dépôt et à la diffusion de documents scientifiques de niveau recherche, publiés ou non, émanant des établissements d'enseignement et de recherche français ou étrangers, des laboratoires publics ou privés.

1 **RAPID REPORT**

2 **Class III peroxidases PRX01, PRX44, and PRX73 potentially target extensins during**  
3 **root hair growth in *Arabidopsis thaliana***

4  
5 Eliana Marzol<sup>1,#</sup>, Cecilia Borassi<sup>1,#</sup>, Philippe Ranocha<sup>2</sup>, Ariel. A. Aptekman<sup>3,4</sup>, Mauro Bringas<sup>5</sup>, Janice  
6 Pennington<sup>6</sup>, Julio Paez-Valencia<sup>6</sup>, Mariana Carignani Sardoy<sup>1</sup>, Javier Martínez Pacheco<sup>1</sup>, Diana R.  
7 Rodríguez-García<sup>1</sup>, Yossmayer del Carmen Rondón Guerrero<sup>1</sup>, Mariana Carignani Sardoy<sup>1</sup>, Juan  
8 Manuel Peralta<sup>1</sup>, Margaret Fleming<sup>7</sup>, John W. Mishler-Elmore<sup>8</sup>, Francisca Blanco-Herrera<sup>9,10</sup>, Patricia  
9 Bedinger<sup>7</sup>, Christophe Dunand<sup>2</sup>, Luciana Capece<sup>5</sup>, Alejandro D. Nadra<sup>3,4</sup>, Michael Held<sup>8</sup>, Marisa S.  
10 Otegui<sup>6,11</sup> & José M. Estevez<sup>1,9,†</sup>

11  
12 <sup>1</sup>Fundación Instituto Leloir and IIBBA-CONICET. Av. Patricias Argentinas 435, Buenos Aires  
13 C1405BWE, Argentina.

14 <sup>2</sup>Université de Toulouse, UPS, UMR 5546, Laboratoire de Recherche en Sciences Végétales, F-31326  
15 CNRS, UMR 5546 Castanet-Tolosan, France.

16 <sup>3</sup>Departamento de Fisiología, Biología Molecular y Celular, Instituto de Biociencias, Biotecnología y  
17 Biología Traslacional (iB3). Facultad de Ciencias Exactas y Naturales, Universidad de Buenos Aires,  
18 Ciudad Universitaria, Buenos Aires C1428EGA, Argentina.

19 <sup>4</sup>Departamento de Química Biológica, Facultad de Ciencias Exactas y Naturales, Universidad de  
20 Buenos Aires (IQUIBICEN-CONICET), Ciudad Universitaria, Buenos Aires C1428EGA, Argentina.

21 <sup>5</sup>Departamento de Química Inorgánica, Analítica y Química Física, Facultad de Ciencias Exactas y  
22 Naturales, Universidad de Buenos Aires (INQUIMAE-CONICET), Buenos Aires, CP. C1428EGA,  
23 Argentina.

24 <sup>6</sup>Laboratory of Cell and Molecular Biology, University of Wisconsin, Madison, WI, USA.

25 <sup>7</sup>Department of Biology, Colorado State University, Fort Collins, Colorado 80523-1878, USA.

26 <sup>8</sup>Department of Chemistry and Biochemistry, Ohio University, Athens, OH 45701, USA.

27 <sup>9</sup>Centro de Biotecnología Vegetal, Facultad de Ciencias de la Vida, Universidad Andrés Bello and  
28 ANID - Millennium Science Initiative Program - Millennium Institute for Integrative Biology (iBio) and  
29 Millennium Nucleus for the Development of Super Adaptable Plants (MN-SAP), Santiago, Chile.

30 <sup>10</sup>Center of Applied Ecology and Sustainability (CAPES), Chile.

31 <sup>11</sup>Departments of Botany and Genetics, University of Wisconsin, Madison, WI, USA.

32  
33 #co-first authors

34 † Correspondence should be addressed. Email: [jestevez@leloir.org.ar](mailto:jestevez@leloir.org.ar) / [jose.estevez@unab.cl](mailto:jose.estevez@unab.cl) (J.M.E).

35  
36 Key words: Arabidopsis, cell walls, extensins, root hairs, ROS, class-III peroxidases.

37 Word count: 4,295

38  
39  
40  
41  
42  
43  
44  
45  
46  
47  
48  
49  
50  
51  
52  
53  
54  
55  
56  
57  
58  
59  
60

**Abstract**

- Root hair cells are important sensors of soil conditions. Expanding several hundred times their original size, root hairs grow towards and absorb water-soluble nutrients. This rapid growth is oscillatory and is mediated by continuous remodelling of the cell wall. Root hair cell walls contain polysaccharides and hydroxyproline-rich glycoproteins including extensins (EXTs).
- Class-III peroxidases (PRXs) are secreted into the apoplastic space and are thought to trigger either cell wall loosening, mediated by oxygen radical species, or polymerization of cell wall components, including the Tyr-mediated assembly of EXT networks (EXT-PRXs). The precise role of these EXT-PRXs is unknown.
- Using genetic, biochemical, and modeling approaches, we identified and characterized three root hair-specific putative EXT-PRXs, PRX01, PRX44, and PRX73. The triple mutant *prx01,44,73* and the PRX44 and PRX73 overexpressors had opposite phenotypes with respect to root hair growth, peroxidase activity and ROS production with a clear impact on cell wall thickness.
- By measuring contrasting levels of cell wall insolubilization of an EXT fluorescent reporter in the triple mutant *prx01,44,73* and in 35S:PRX44, we suggest that these three putative EXT-PRXs control EXT-mediated cell wall properties during the polar expansion of root hair cells.

Word count: 188

61

## 62 **Introduction**

63 Primary cell walls, composed by a diverse network containing mainly polysaccharides and a small  
64 amount of structural glycoproteins, regulate cell elongation, which is crucial for several plant growth  
65 and developmental processes. Extensins (EXTs) belong to hydroxyproline (Hyp)-rich glycoprotein  
66 (HRGP) superfamily and broadly include related glycoproteins such as proline-rich proteins (PRPs)  
67 and leucine-rich repeat extensins (LRXs) with multiple Ser-(Pro)<sub>3-5</sub> repeats that may be *O*-  
68 glycosylated and contain Tyr (Y)-based motifs (Lamport et al. 2011; Marzol et al. 2018). EXTs require  
69 several modifications before they become functional (Lamport et al., 2011; Marzol et al. 2018). After  
70 being hydroxylated and *O*-glycosylated in the secretory pathway, the secreted *O*-glycosylated EXTs  
71 are crosslinked and insolubilized in the plant cell wall by the oxidative activity of secreted class-III  
72 peroxidases (PRXs) on the Tyr-based motifs (Baumberger 2001, 2003; Ringli 2010; Held et al. 2004;  
73 Lamport et al., 2011; Chen et al. 2015; Marzol et al. 2018). PRXs are thought to facilitate both intra  
74 and inter-molecular covalent Tyr–Tyr crosslinks in EXT networks, possibly through the assembly of  
75 triple helices (Velasquez et al. 2015a; Marzol et al. 2018) by generating *isodityrosine* units (IDT) and  
76 *pulcherosine*, or *di-isodityrosine* (Di-IDT), respectively (Brady et al., 1996; 1998; Held et al. 2004). In  
77 addition, *O*-glycosylation levels in EXTs also affect their insolubilization process in the cell wall (Chen  
78 et al. 2015; Velasquez et al. 2015a) since it might influence the EXT interactions with other cell wall  
79 components (Nuñez et al., 2009; Valentin et al., 2010). However, the underlying molecular  
80 mechanisms of EXT crosslinking and assembly have not been fully determined. It is proposed that *O*-  
81 glycosylation levels as well as the presence of Tyr-mediated crosslinking in EXT and related  
82 glycoproteins allow them to form a dendritic glycoprotein network in the cell wall. This EXT network  
83 affects *de novo* cell wall formation during embryo development (Hall and Cannon 2002; Cannon *et*  
84 *al.*, 2008), they are also implicated in roots, petioles and rosette leaves growth (Saito et al 2014;  
85 Møller et al. 2017) and in polar cell expansion processes in root hairs (Baumberger 2001, 2003;  
86 Ringli 2010; Velasquez et al. 2011; 2012; 2015a,b) as well as in pollen tubes (Fabrice et al. 2018;  
87 Sede et al. 2018; Wang et al. 2018).

88

89 Apoplastic class-III PRXs are heme-iron-dependent proteins, members of a large multigenic family in  
90 land plants, with 73 members in *Arabidopsis thaliana* (Passardi et al. 2004; Weng and Chapple,  
91 2010). These PRXs catalyze several different classes of reactions. PRX activities coupled to *apo*ROS  
92 molecules (*apo*H<sub>2</sub>O<sub>2</sub>) directly affect the degree of cell wall crosslinking (Dunand et al. 2007) by  
93 oxidizing cell wall compounds and leading to stiffening of the cell wall through a peroxidative cycle  
94 (PC) (Passardi et al. 2004, Cosio & Dunand 2009; Lamport et al. 2011). By contrast, *apo*ROS coupled to  
95 PRX activity enhances non-enzymatic cell wall-loosening by producing oxygen radical species (e.g.,  
96 •OH) and promoting growth in the hydroxylic cycle (HC). In this HC cycle, PRXs catalyze the reaction  
97 in which hydroxyl radicals (•OH) are produced from H<sub>2</sub>O<sub>2</sub> after O<sub>2</sub>•<sup>-</sup> dismutation. In this manner,  
98 some PRXs (e.g. PRX36) may function in weaken plant cell walls by the generated •OH that cleave

99 cell wall polysaccharides in seed mucilage extrusion in epidermal cells in the *Arabidopsis* seed coat  
100 (Kunieda et al., 2013). It is unclear how these opposite effects on cell wall polymers are coordinated  
101 during plant growth (Passardi et al. 2004, Cosio & Dunand 2009; Lee et al. 2013; Ropollo et al. 2011;  
102 Lee et al 2018; Francoz et al. 2019). Finally, PRXs also contribute to the superoxide radical ( $O_2^{\bullet-}$ ) pool  
103 by oxidizing singlet oxygen in the oxidative cycle (OC), thereby affecting  $apoH_2O_2$  levels. Thus, several  
104 PRXs are involved in the oxidative polymerization of monolignols in the apoplast of the lignifying  
105 cells in xylem (e.g. PRX17, Cosio et al 2017; PRX72, Herrero et al. 2013), in the root endodermis (e.g.  
106 PRX64; Lee et al. 2013; Ropollo et al. 2011), and in petal detachment (Lee et al 2018). In addition,  
107 PRXs are able to polymerize other components of the plant cell wall such as suberin (Bernards et al.,  
108 1999) and EXTs (Schnabelrauch *et al.*, 1996; Jackson et al., 2001). Although several candidates of  
109 PRXs have been associated specifically with EXT-crosslinking (EXT-PRXs) by *in vitro* studies  
110 (Schnabelrauch et al., 1996; Wojtaszek et al., 1997; Jackson et al., 2001; Price et al., 2003; Pereira et  
111 al. 2011; Dong et al., 2015) or based on an immunolabelling extensin study linked to a genetic  
112 profile (Jacobowitz et al. 2019), the *in vivo* characterization and mode of action of these EXT-PRXs  
113 remain largely unknown. Recently, PRX62 and PRX69 were identified as key apoplastic PRXs that  
114 modulate ROS-homeostasis and cell wall EXT-insolubilization linked to RH elongation at low  
115 temperature (Martínez Pacheco et al. 2022). In addition, PRX44 was involved in ROS accumulation  
116 linked to the root hair initiation process (Martin et al. 2022). In this line, in *Arabidopsis* roots, the  
117 responses mediated by ethylene and auxin signaling pathways might involve class-III PRXs-  
118 dependent cell wall modifications during cell expansion (Mangano et al. 2017; Mangano et al. 2019;  
119 Pereira et al. 2022). In this work, we used a combination of reverse genetics, molecular and cell  
120 biology, computational molecular modeling, and biochemistry to identify three apoplastic PRXs,  
121 PRX01, PRX44 and PRX73, as key enzymes potentially involved in Tyr-crosslinking of cell wall EXTs in  
122 growing root hair cells. In addition, we propose a hypothetical model in which O-glycosylation levels  
123 on the triple helixes of EXTs might regulate the degree of Tyr-crosslinking affecting the expansion  
124 properties of cell walls as suggested before based on the extended helical polyproline-II  
125 conformation state of EXTs (Stafstrom & Staehelin 1986; Owen et al., 2010; Ishiwata et al., 2014)  
126 together with an experimental Atomic Force Microscopic (AFM) analysis of crosslinked EXT3  
127 monomers (Cannon et al. 2008) linked to modelling approaches (Velasquez et al. 2015a; Marzol et al  
128 2018). Our results open the way for the discovery of similar interactions in EXT assemblies during  
129 root hair development and in response to the environmental changes, such fluctuating nutrient  
130 availability in the soil.

131

## 132 **Results**

133 In this work, we have chosen to analyze root hair cells because they are an excellent model for  
134 tracking cell elongation and identifying PRXs involved in EXT assembly. In previous work, the  
135 phenotypes of mutants for PRX01, PRX44 and PRX73 suggested that these PRXs are involved in root  
136 hair growth and ROS homeostasis, although their mechanisms of action remained to be

137 characterized (Mangano et al. 2017). All three PRXs are under the transcriptional regulation of the  
138 root hair specific transcription factor RSL4 (Yi et al. 2010; Mangano et al. 2017). As expected, these  
139 three PRXs are also highly co-expressed with other root hair-specific genes encoding cell wall EXTs  
140 (e.g., EXT6-7, EXT12-14, and EXT18) and EXT-related glycoproteins (e.g. LRX1 and LRX2), which  
141 functions in cell expansion (Ringli 2010; Velasquez et al. 2011; Velasquez et al. 2015b) (**Figure S1**).  
142 Based on this evidence, we hypothesized that these three PRXs might be EXT-PRXs and catalyze Tyr-  
143 crosslinks to assemble EXTs in root hair cell walls.

144  
145 To validate that PRX01, PRX44, and PRX73 are expressed specifically in root hairs, we made  
146 transcriptional reporters harboring GFP-tagged fusions of the promoter regions of their genes. In  
147 agreement with the *in silico* database (Mangano et al. 2017 and **Figure S1**), all three genes were  
148 strongly expressed in root hair cells during cell elongation (**Figure 1A**). Single mutants for these  
149 three PRXs showed almost normal root hair growth (Mangano et al. 2017), suggesting a high degree  
150 of functional redundancy. Double combinations of *prx44 prx73* (Mangano et al. 2017), *prx01 prx44*  
151 and *prx01 prx73* (this study, not shown) as well as the triple null mutant, *prx01 prx44 prx73*  
152 (*prx01,44,73*) showed similarly shorter root hair cells (**Figure 1B**) than what was previously reported  
153 for each of the individual *prx* mutants (Mangano et al. 2017). We also obtained two independent  
154 lines for each overexpressing PRXs fused to GFP and under the control of a strong *35SCaMV*  
155 promoter (PRX<sup>OE</sup>). Unlike the *prx01,44,73* triple mutant, the lines overexpressing PRX44 and PRX73  
156 had significantly longer root hairs than the Wt Col-0 control (**Figure 2A–B**). The root hairs of the  
157 PRX01<sup>OE</sup> lines, however, were similar to those of Wt Col-0 (**Figure 2A–B**). We reasoned that the lack  
158 of enhanced root hair expansion in the PRX01<sup>OE</sup> lines could be due to reduced levels of  
159 overexpression compared to the PRX44<sup>OE</sup> and PRX73<sup>OE</sup> lines. However, based on the GFP signals in  
160 intact roots (**Figure 2C**), we established that PRX01<sup>OE</sup> and PRX44<sup>OE</sup> are strongly expressed, whereas  
161 PRX73<sup>OE</sup> showed more moderate expression. The lack of root hair growth enhancement in PRX01<sup>OE</sup>  
162 line might be due to regulatory aspects on the protein activity rather than in the protein level. Then,  
163 we tested if a single peroxidase when overexpressed is able to rescue the triple mutant *prx01,44,73*.  
164 Only PRX44<sup>OE</sup>, but not PRX01<sup>OE</sup> and PRX73<sup>OE</sup>, was able to restore root hair growth to almost the Wt  
165 Col-0 levels (**Figure 2D**). Together, these results highlight the partially redundant roles of PRX01,  
166 PRX44, and PRX73 as positive regulators of polar growth. At the same time, they showed some  
167 differences in their effect when overexpressed. This is in agreement with the negative effect of  
168 SHAM (salicylic hydroxylamino acid), a peroxidase activity inhibitor (Ikeda-Saito, Shelley et al. 1991;  
169 Davey and Fenna 1996), on root hair growth (Mangano et al. 2017). Here is important to highlight  
170 that a SHAM treatment produces a more drastic effect on root hair growth and on the inhibition of  
171 overall peroxidase activity in the roots (Mangano et al. 2017) than the triple mutant *prx01 prx44*  
172 *prx73*, suggesting the implication of other unidentified PRXs.

173

174 To confirm that our mutant and overexpressing lines had the expected changes in peroxidase  
175 activity, we measured *in vitro* total peroxidase activity using a guaiacol oxidation-based assay. The  
176 *prx01,44,73* roots showed reduced peroxidase activity (close to 50% reduction) (**Figure 1C**), whereas  
177 there was a 40–50% increase in PRX73<sup>OE</sup> and an approximately 20% increase in PRX44<sup>OE</sup> (**Figure 2E**).  
178 Consistent with our root hair growth analysis (**Figure 2A**), PRX01<sup>OE</sup> showed Wt col-0 peroxidase  
179 activity (**Figure 2E**). The homeostasis and levels of ROS (mostly H<sub>2</sub>O<sub>2</sub>) that regulates polar growth of  
180 root hair cells (Mangano et al. 2017) is composed by apoplastic ROS (<sub>apo</sub>ROS) as well as by the  
181 cytoplasmic ROS pool (<sub>cyt</sub>ROS). Both pools of ROS, their homeostasis and levels are modulated by  
182 their transport from the apoplast to the cytoplasmic side by specific aquaporins (PIPs for plasma  
183 membrane intrinsic proteins) in plant cells (Dynowski et al., 2008; Hooijmaijers et al., 2012  
184 Rodrigues et al. 2017). We hypothesized that these three PRXs might change the levels of ROS, most  
185 probably H<sub>2</sub>O<sub>2</sub>, for their catalytic functions in the cell wall/apoplast. Therefore, we measured <sub>cyt</sub>ROS  
186 levels by oxidation of H<sub>2</sub>DCF-DA and <sub>apo</sub>ROS levels with the Amplex Ultra Red (AUR) probe in root  
187 hair tips. The *prx01,44,73* root hair tips showed lower levels of <sub>cyt</sub>ROS (**Figure 1D**) but increased  
188 <sub>apo</sub>ROS accumulation (**Figure 1E**) compared to Wt Col-0. The <sub>apo</sub>ROS levels were similar in PRX01<sup>OE</sup>,  
189 and slightly lower in PRX44<sup>OE</sup>, and PRX73<sup>OE</sup> lines when compared to Wt Col-0 (**Figure 2F**). These  
190 results suggest that PRX01, PRX44, and PRX73 function as apoplastic regulators of ROS-linked root  
191 hair cell elongation.

192  
193 Next, to further analyze the ultrastructure of the cell wall in growing root hairs, we analyzed Wt Col  
194 and *prx01,44,73* triple mutant roots treated or not with SHAM by transmission electron microscopy  
195 (**Figure 3A**). Much found thinner cell walls at the root hair tips of *prx01,44,73* ( $0.61 \pm \text{SD } 0.14 \mu\text{m}$ )  
196 when compared to Wt Col-0 plants ( $1.2 \pm \text{SD } 0.3 \mu\text{m}$  for Wt) (**Figure 3B**). SHAM treatment caused a  
197 statistically significant increase in cell wall thickness in *prx01,44,73* root hairs (**Figure 3B**), but not in  
198 Wt Col-0. This result suggests the importance of peroxidase activity in cell wall structure and  
199 highlights that depletion of these three PRXs PRX01, PRX44, PRX73 (in the triple mutant) results in  
200 an overall reduction in cell wall thickness in growing root hairs. This implies that mis-regulation of  
201 PRX activity (reduced/impaired function) affects the capacity of root hairs to form normal cell walls  
202 and this clearly affects their cell expansion process. Then, we designed an EXT reporter to track EXT  
203 secretion and PRX-mediated insolubilization in the cell walls during root hair cell elongation. The  
204 secreted EXT reporter carries a Tomato tag (SS-TOM-Long-EXT) that is fluorescent under the acidic  
205 pH (Shen et al. 2014) that is typical of plant cell walls and apoplastic spaces (Stoddard & Rolland  
206 2018). A secreted Tomato tag (ss-TOM) was used as a control (**Figure S2A**). The EXT domain includes  
207 two Tyr, which are at the C-terminus and separated by 10 amino acids (Stratford et al., 2001).  
208 Expression of the EXT reporter was first tested in onion (*Allium cepa*) cells, and then the reporter  
209 was stably expressed in Arabidopsis root hairs (**Figure S2C-F**). In both cases, plasmolysis was used to  
210 retract the plasma membrane from the cell surface to show that the EXT reporter was localized in  
211 the cell walls. Using immunoblot analysis, we detected the full-length EXT-Tomato fusion protein,

212 with possible *O*-glycan modifications, running as higher molecular weight bands than expected  
213 (**Figure S2B**). Importantly, the EXT reporter did not interfere with the polar growth of root hairs  
214 (**Figure S2D**), and, therefore, it could be used to track changes in the *in situ* arrangement of cell wall  
215 EXTs. SS-TOM-Long-EXT is clearly secreted in the cell wall of growing root hairs (**Figure S2C**). Then,  
216 we tested if these EXT reporter insolubilization is affected in *prx01,44,73* triple mutant background  
217 and in 35S:PRX44. In both cases, we were able to detect different levels of SS-EXT-LONG TOM  
218 insolubilization, higher in the *prx01,44,73* triple mutant background and slightly lower in the  
219 35S:PRX44. This suggests that changes in the peroxidase environment due to the suppression of  
220 several PRXs or the enhancement of a single PRX, the cell wall insolubilization of SS-EXT-LONG  
221 reporter was modified. This is also in agreement with the drastic changes in cell wall thickness in the  
222 *prx01,44,73* triple mutant by TEM (**Figure 3**).

223  
224 We then assessed the level of crosslinking of EXT Tyr residues by measuring peptidyl-tyrosine (Tyr)  
225 and isodityrosine (IDT, dimerized Tyr) in EXT extracted from whole roots. We detected a significant  
226 increase in peptidyl-Tyr in the *prx01,44,73* triple mutant relative to Wt Col-0, and slightly higher  
227 levels of IDT in EXTs extracted from the PRX73<sup>OE</sup> line (**Table 1**). By contrast, we identified strong  
228 downregulation of Tyr- and IDT-levels in the EXT under-*O*-glycosylation mutants *p4h5 sergt1-1*, and  
229 *sergt1-1 rra3* (**Table 1**). In these two double mutants, root hair growth is drastically inhibited  
230 (Velasquez et al. 2015a). PROLYL 4-HYDROXYLASE (P4H5), PEPTIDYL-SER GALACTOSYLTRANSFERASE  
231 (SGT1/SERGT1), and REDUCE RESIDUAL ARABINOSE 3 (RRA3) are key enzymes that modify EXT  
232 hydroxylation (P4H5) and EXT *O*-glycosylation (SERGT1 and RRA3) (Marzol et al. 2018). Specifically, it  
233 was shown that P4H5 is a 2-oxoglutarate (2OG) dioxygenase that catalyzes the formation of trans-4-  
234 hydroxyproline (Hyp/O) from peptidyl-proline preferentially in an EXT context allowing these  
235 proteins to be *O*-glycosylated (Velasquez et al. 2011; Velasquez et al. 2015b). In the case of RRA3,  
236 together with RRA1–RRA2 homologous proteins (Egelund et al., 2007; Velasquez et al., 2011), they  
237 are thought to transfer the second arabinose to the sort glycan (composed by 4–5 units of L-  
238 arabinofuranose) attached to the Hyp in the EXT peptides. SERGT1 add the single galactose units to  
239 the serine in the repetitive motif of Ser-(Pro)<sub>3–5</sub> present in EXT and EXT-related proteins (Saito et al.  
240 2014). These results are consistent with the notion that *O*-glycans strongly affect EXT Tyr  
241 crosslinking, as was previously suggested based on the drastically reduced root hair growth of the  
242 under-glycosylation mutants and *in vitro* crosslinking rates (Velasquez et al 2015a,b; Chen et al.  
243 2015). We hypothesize that absent or low *O*-glycosylation of EXTs or an increase in PRX levels may  
244 trigger a reduction in the amount of peptidyl-Tyr and IDT levels in EXTs, with a putative concomitant  
245 increase in the amounts of higher-order Tyr crosslinks (trimers as Pulcherosine and tetramers as Di-  
246 IDT), thus inhibiting root hair growth. For technical reasons we could not measure the Pulcherosine  
247 and Di-IDT levels described before in EXTs (Brady et al., 1996; 1998; Held et al. 2004) to test this  
248 hypothesis. Further research is needed to decipher the *in vivo* regulation of Tyr crosslinking of EXTs  
249 by these three PRXs in plant cells.

250  
251 A major limitation in our understanding of how EXTs function in plant cell walls is the lack of a  
252 realistic full-length EXT protein model. We used coarse-grained molecular dynamics to build a larger  
253 model of a triple-helix EXT sequence that includes 10 conserved repeats  
254 (SPPPPYVYSSPPPPYVYSSPKVYYK, 250 aminoacids in each polypeptide chain) (**Figure S3A–B**).  
255 Parameters for the *O*-glycosylated form of EXT were developed in this work (**Figure S4**). The EXT  
256 molecules were modeled in two different states: as a non-glycosylated trimeric helical conformation  
257 similar to animal collagen and in the *O*-glycosylated state, with 4 arabinose monosaccharides in each  
258 hydroxyproline. Those two states were simulated restraining both ends of the polypeptide chains, to  
259 model a fully extended helix (consistent with an “indefinitely long-EXT”), and without that  
260 restriction, to evaluate the conformation that an isolated 10-repeat triple helix would adopt. The  
261 results indicate the importance of the triple-helix conformation in the overall stability of the protein  
262 and especially in the conservation of its fibril-like structure, in agreement with shorter-repeats single  
263 helix simulations performed previously (Velasquez et al. 2015a; Marzol et al. 2018). The total  
264 volume of the extended systems triple helix was measured in both glycosylation states (**Table S1**),  
265 differentiating EXT-protein-only and EXT-protein+glycan volumes for the fully *O*-glycosylated EXT  
266 state. We observed that the EXT-protein-only volume was significantly augmented by the presence  
267 of the oligosaccharide moieties, indicating that *O*-glycans increase the distance between peptide  
268 chains in the EXT triple helix. We report the average diameters for those systems (**Table S1**), which  
269 are consistent with the diameters previously reported based on Atomic Force Microscopy (AFM)  
270 images (Cannon et al. 2008). Additionally, *O*-glycosylation contributes to an increase in the average  
271 distance between the side chains of tyrosine residues, decreasing the proportion of tyrosine side  
272 chains that are close enough to lead to crosslinked EXT chains (**Figure S3C**). Current experimental  
273 and modeling lines of evidence are in agreement with the proposed role of proline-hydroxylation  
274 and carbohydrate moieties in keeping the EXT molecule in an extended helical polyproline-II  
275 conformation state (Stafstrom & Staehelin 1986; Owen et al., 2010; Ishiwata et al., 2014). This  
276 extended conformation might allow EXTs to interact properly with each other and with other  
277 components in the apoplast, including PRXs and pectins, to form a proper cell wall network (Nuñez  
278 et al., 2009; Valentin et al., 2010).

279  
280 To test if these three PRXs (PRX01, PRX44, and PRX73) might be able to interact with single-chain  
281 EXTs, we performed homology modeling with GvEP1, an EXT-PRX that is able to crosslink EXTs *in*  
282 *vitro* (Jackson et al., 2001; Pereira et al. 2011). In addition, we included PRX64, as a PRX described  
283 for lignin polymerization in the root endodermis (Lee et al. 2013) and PRX36, which is able to bind  
284 homogalacturonan pectin in the seed coat (Francoz et al. 2019) as controls. By *docking* analysis, we  
285 obtained interaction energies (Kcal/mol) for all of them. We analyzed docking with four different  
286 short EXT peptides: a non-hydroxylated peptide, a hydroxylated peptide, an arabinosylated peptide  
287 and an arabino-galactosylated peptide. As mentioned earlier, it was previously shown that mutants

288 carrying under-*O*-glycosylated EXTs have severe defects in root hair growth (Velasquez et al. 2011;  
289 Velasquez et al. 2015a). Our docking results for the different PRXs show consistent interaction  
290 energy differences that depend on the EXT glycosylation state, being higher for non-*O*-glycosylated  
291 species. In addition, *O*-glycosylated EXT variants docked in a rather dispersed way while non-*O*-  
292 glycosylated variants preferentially docked in a grooved area (**Figure S5A–C**). Furthermore, **Figure**  
293 **S5A** shows how a non-*O*-glycosylated peptide binds through a groove, leaving one Tyr docked in a  
294 cavity and very close to the heme iron (5Å), with a second Tyr a few Angstroms away. The  
295 arrangement and distances between the tyrosines suggest that this could be an active site where  
296 Tyr crosslinking takes place. Although it is not possible to compare the interaction energies obtained  
297 with the different EXT species among docking runs, a general trend can be observed in **Figure S5C**. In  
298 general, we observed higher interaction energies (more negative values) for hydroxylated EXT  
299 species, followed by non-hydroxylated EXTs, and then by *O*-glycosylated EXT variants. When we  
300 compared interaction energies among different PRXs interacting with EXT substrates with the same  
301 degree of *O*-glycosylation, we observed that PRX73 displayed the highest interaction activity with  
302 the non-hydroxylated EXT species, followed by PRX01 and then PRX44. For the hydroxylated EXT  
303 variant, the order was PRX44>PRX73>PRX01. PRX44 displayed the highest interaction energy with  
304 the *O*-glycosylated species. All together, these results are consistent with the constitutive root hair  
305 growth effect observed for PRX44<sup>OE</sup> and PRX73<sup>OE</sup> and with non-glycosylated EXT being the substrate  
306 of peroxidation. Overall, this possibly indicates that PRX44 and PRX73 might interact with EXT  
307 substrates and possibly catalyze Tyr-crosslinking in open regions of the EXT backbones with little or  
308 no *O*-glycosylation. This is in agreement with previous studies that suggested that high levels of *O*-  
309 glycosylation in certain EXT segments physically restrict EXT lateral alignments, possibly by acting as  
310 a branching point (Cannon et al.2008; Velasquez et al., 2015a; Marzol et al. 2018).

311  
312 To examine the evolution of PRX01, PRX44, and PRX73, we performed comprehensive phylogenetic  
313 analyses of Class-III peroxidases across diverse land plant lineages. Under low selective pressure to  
314 maintain substrate specificity, EXT-PRX activities might have evolved multiple times in parallel  
315 during land plant evolution through gene duplication followed by neofunctionalization or  
316 subfunctionalization. PRX01, PRX44, and PRX73 belong to three independent orthologous groups  
317 (**Figure S6**) and orthologs for each *A. thaliana* PRX have been detected in available Brassicaceae  
318 genomes and in various Angiosperm and Gymnosperm families, but not from Lycophytes and from  
319 non-vascular land plants. Thus, these three PRX sequences were the result of ancestral duplications  
320 before the divergence between Gymnosperms and Angiosperms but after the emergence of the  
321 Tracheophytes (**Figure S6**). Orthologs of the three PRX genes have only been detected in true root  
322 containing organisms and these three PRXs are expressed in roots and root hairs, as are most of  
323 their orthologous sequences (where expression data are available) (**Figure S7**). This strongly  
324 supports the hypothesis that the three independent orthogroups have conserved functions in roots.  
325 With the exception of PRX73, which belongs to a cluster containing the putative EXT-PRX from

326 tomato (*Solanum lycopersicum*; LePRX38), the other two PRX sequences did not cluster with  
327 sequences already described as putative EXT-PRXs, such as PRX09 and PRX40 (Jacobowitz et al.  
328 2019). Indeed, the other known EXT-PRXs (identified mostly based on *in vitro* evidence) are not  
329 clustered together, but are widely distributed in the tree (**Figure S7**). This analysis suggests that  
330 plant EXT-PRXs might have evolved several times in parallel during Tracheophyte evolution.

331

## 332 **Discussion**

333 Based on the results shown in this work, we propose a working model in which PRX01, PRX44, and  
334 PRX73 (and possibly other PRXs) control root hair growth by channelling H<sub>2</sub>O<sub>2</sub> consumption and  
335 affecting the cell wall hardening process. In this polar growing cells, it is known that H<sub>2</sub>O<sub>2</sub> is primary  
336 derived from by the respiratory burst oxidase homolog C (RBOHC), and to a lower extent from  
337 RBOHH and RBOHJ activities that produce superoxide ions (Monshauser et al. 2007; Tajeda et al.  
338 2008; Mangano et al. 2017) that are further converted chemically or enzymatically to H<sub>2</sub>O<sub>2</sub>. Then,  
339 part of H<sub>2</sub>O<sub>2</sub> might be transported from the apoplast to the cytoplasm side by specific PIPs as it was  
340 shown to occur in several plant cell types (e.g. in stomata and epidermal cells) in response to diverse  
341 stimuli (Dynowski et al., 2008; Hooijmaijers et al., 2012; Rodrigues et al. 2017). When apoplastic PRX  
342 protein levels are low, which is linked to reduced peroxidase activity as in the triple mutant  
343 *prx01,44,73*, high levels of H<sub>2</sub>O<sub>2</sub> accumulate in the apoplast, triggering through the oxidative cycle  
344 (OC) a cell wall loosening effect that affects growth homeostasis and inhibits expansion by  
345 decreasing root hair growth and cell wall thickness (**Figure S8**). Concomitantly, deficient PRX activity  
346 in the apoplast also triggers lower H<sub>2</sub>O<sub>2</sub> levels in the cytoplasm of growing root hairs. This is in  
347 agreement with the fact that exogenously supplied H<sub>2</sub>O<sub>2</sub> inhibited root hair polar expansion,  
348 whereas treatment with ROS scavengers (e.g., ascorbic acid) caused root hair bursting (Orman-ligeza  
349 et al. 2016), reinforcing the notion that *apo*ROS modulates cell growth by impacting cell-wall  
350 properties (Mangano et al. 2017). Our results suggest that either low or high levels of apoplastic  
351 Class-III PRXs in the root hair cell walls might affect the ROS-homeostasis and cell wall assemblage  
352 with a clear effect on cell expansion. Changes in ROS-homeostasis produced by altered levels of  
353 these PRXs in the apoplast might affect the secretion, targeting and, possibly the crosslinking of cell  
354 wall components including EXTs, affecting RH cell elongation.

355

356 Currently, most of the 73 apoplastic Class-III PRXs in *Arabidopsis thaliana* have no assigned  
357 biological function. In this work, we have characterized three related EXT-PRXs, PRX01, PRX44, and  
358 PRX73 that function in ROS homeostasis and potentially in EXT assembly during root hair growth.  
359 These PRXs might control Tyr crosslinking in EXTs and related glycoproteins and modify its secretion  
360 and assembly in the nascent tip cell walls. Using modeling and docking approaches, we were able to  
361 measure the interactions of these PRXs with single chain EXT substrates. All these lines of evidence  
362 indicate that PRX01, PRX44, and PRX73 are important enzymes that could be involved in EXT  
363 assembly during root hair growth. In a similar manner, PRX62 and PRX69 were identified as key

364 apoplastic PRXs that modulate ROS-homeostasis and cell wall EXT-insolubilization linked to RH  
365 elongation at low temperature (Martínez Pacheco et al. 2022). Collectively, it is starting to emerge a  
366 predominant role of ROS-homeostasis partially regulated by specific PRXs as a key component in  
367 polar RH elongation. From an evolutionary perspective, all the putative EXT-PRXs (previously  
368 identified based on *in vitro* evidence or immunolabeling) do not cluster together in the phylogenetic  
369 tree of Class-III PRXs, suggesting that plant-related EXT-PRXs might have evolved several times in  
370 parallel during Tracheophyte evolution. Interestingly, as a convergent evolutionary extracellular  
371 assembly, hydroxyproline-rich collagen Class-IV, similar to the green EXT lineage and related  
372 glycoproteins, is also crosslinked by the activity of a specific class of animal heme peroxidases  
373 (named peroxidasin or PXDN) to form insoluble extracellular networks (Vanacore et al. 2009; Bhave  
374 et al. 2012). While the biophysical properties of collagen IV allow the correct development and  
375 function of multicellular tissues in all animal phyla (Brown et al. 2017), EXT assemblies also have key  
376 functions in several plant cell expansion and morphogenesis processes (Baumberger 2001, 2003;  
377 Hall and Cannon et al. 2002; Cannon *et al.*, 2008; Ringli 2010; Lamport et al., 2011; Velasquez et al.  
378 2015a,b; Fabrice et al. 2018; Sede et al. 2018; Marzol et al. 2018). This might imply that crosslinked  
379 extracellular matrices based on hydroxyproline-rich polymers (e.g., collagens and EXTs) have  
380 evolved more than once during eukaryotic evolution, providing mechanical support to single and  
381 multiple cellular tissues. Further analyses are required to establish how these described EXT-PRXs  
382 catalyze Tyr crosslinks on EXTs at the molecular level and how this assembly process is regulated  
383 during polar cell expansion.

384

## 385 **Experimental Procedures**

386

387 **Plant and growth conditions.** *Arabidopsis thaliana* Columbia-0 (Col-0) was used as the wild Class  
388 (Wt) genotype in all experiments. All mutants and transgenic lines tested are in this genetic  
389 background. Seedlings were germinated on agar plates in a Percival incubator at 22°C in a growth  
390 room with 16h light/8h dark cycles for 10 days at 140  $\mu\text{mol m}^{-2}\text{s}^{-1}$  light intensity. Plants were  
391 transferred to soil for growth under the same conditions. For identification of T-DNA knockout lines,  
392 genomic DNA was extracted from rosette leaves. Confirmation by PCR of a single and multiple T-  
393 DNA insertions in the target PRX genes were performed using an insertion-specific LBb1.3 primers in  
394 addition to one gene-specific primer. To ensure gene disruptions, PCR was also run using two gene-  
395 specific primers, expecting bands corresponding to fragments larger than in WT. We isolated  
396 homozygous lines for PRX01 (AT1G05240, *prx01-2*, Salk\_103597), PRX44 (AT4G26010, *prx44-2*,  
397 Salk\_057222) and PRX73 (AT5G67400, *prx73-3*, Salk\_009296). SERGT1 (*sergt1-1* SALK\_054682), *rra3*  
398 (GABI\_233B05) (Velasquez et al., 2011) and *p4h5* T-DNA mutant (Velasquez et al., 2011) were  
399 isolated and described previously. Double and triple mutants were generated by manual crosses of  
400 the corresponding single mutants (Velasquez et al., 2015a). All the mutant lines used in this study  
401 are described in **Table S2**.

402

403 **PRX::GFP and 35S::PRX-GFP lines.** Vectors based on the Gateway cloning technology (Invitrogen)  
404 were used for all manipulations. Constitutive expression of PRXs-GFP tagged lines were achieved in  
405 plant destination vector pMDC83. cDNA PRXs sequences were PCR-amplified with AttB  
406 recombination sites. PCR products were then recombined first in pDONR207 and transferred into  
407 pGWB83. To generate transcriptional reporter, the PRXs promoter regions (2Kb) was amplified and  
408 recombined first in pDONR207 and transferred into pMDC111. All the transgenic lines used in this  
409 study are described in **Table S2**.

410

411 **SS-TOM and SS-TOM-Long-EXT constructs.** The binary vector pART27, encoding tdTomato secreted  
412 with the secretory signal sequence from tomato polygalacturonase and expressed by the  
413 constitutive CaMV 35S promoter (pART-SS-TOM), was the kind gift of Dr. Jocelyn Rose, Cornell  
414 University. The entire reporter protein construct was excised from pART-SS-TOM by digesting with  
415 *NotI*. The resulting fragments were gel-purified with the QIAquick Gel Extraction Kit and ligated  
416 using T4 DNA Ligase (New England Biolabs) into dephosphorylated pBlueScript KS+ that had also  
417 been digested with *NotI* and gel-purified to make pBS-SS-TOM. The plasmid was confirmed by  
418 sequencing with primers 35S-FP (5'-CCTTCGCAAGACCTTCCTC-3') and OCS-RP (5'-  
419 CGTGACAACAGAATTGAAAGC-3'). The sequence of the EXT domain from *SIPEX1* (NCBI accession  
420 AF159296) was synthesized and cloned by GenScript into pUC57 (pUC57-EXT). The plasmid pBS-SS-  
421 TOM-Long-EXT was made by digesting pUC57-EXT and pBS-SS-TOM with *NdeI* and *SgrAI*, followed by

422 gel purification of the 2243 bp band from pUC57-EXT and the 5545 bp band from pBS-SS-TOM, and  
423 ligation of the two gel-purified fragments. The pBS-SS-TOM-Long-EXT plasmid was confirmed by  
424 sequencing with 35S-FP, OCS-RP, and tdt-seq-FP (5'- CCCGTTCAATTGCCTGGT-3'). Both pBS plasmids  
425 were also confirmed by digestion. The binary vector pART-SS-TOM-Long-EXT was made by gel  
426 purifying the *NotI* insert fragment from the pBS-SS-TOM-Long EXT plasmid and ligating it with pART-  
427 SS-TOM backbone that had been digested with *NotI*, gel purified, and dephosphorylated. This  
428 plasmid was confirmed by sequencing. The construct SS-TOM and SS-TOM-Long-EXT were  
429 transformed into *Arabidopsis* plants. The secretory sequence (SS) from tomato polygalacturonase is  
430 MVIQRNSILLIIIIFASSISTCRSGT (2.8kDa) and the EXT-Long domain sequence with six alanine cluster is  
431 BAAAAAAACTLPSLKNFTFSKNIFESMDETCRPSESKQVKIDGNENCLGGRSEQRTEKECFPVVSKPVDCSKGHCG  
432 VSREGQSPKDPKTVTTPPKSTPTTPKPNPSPPPKTLPPPKTSPPPPVHSPPPPVASPPPPVHSPPPPVASPPPP  
433 VHSPPPPVASPPPPVHSPPPPVASPPPPVHSPPPPVHSPPPPVASPPPPVHSPPPPVHSPPPPVHSPPPVHSPPP  
434 PVHSPPPPVASPPPPVHSPPPVHSPPPVHSPPPVHSPPPVHSPPPPVASPPPPVHSPPPPVASPPPPVHSPPPVHSP  
435 PPPVASPPPPVHSPPPVHSPPPVHSPPPVHSPPPVHSPPPVHSPPPVHSPPPVHSPPPVHSPPPVHSPPPVHSP  
436 PPPIFQGY\*395-(39.9kDa). The predicted molecular size for SS-TOM protein is 54.2 kDa and for SS-  
437 TOM-EXT-Long Mw is 97.4 kDa. All the transgenic lines used in this study are described in **Table S2**.

438  
439 **Root hair phenotype.** For quantitative analysis of root hair phenotypes in *prx01,44,73* mutant,  
440 35S:PRX-GFP lines and Wt Col-0, 200 fully elongated root hairs were measured (n roots= 20-30) from  
441 seedlings grown on vertical plates for 10 days. Values are reported as the mean  $\pm$ SD using the Image  
442 J software. Measurements were made after 7 days. Images were captured with an Olympus SZX7  
443 Zoom microscope equipped with a Q-Colors digital camera.

444  
445 **Confocal imaging.** Root hairs were ratio imaged with the Zeiss LSM 710 laser scanning confocal  
446 microscope (Carl Zeiss) using a 40X oil-immersion, 1.2 numerical aperture. EGFP (473–505nm)  
447 emission was collected using a 458-nm primary dichroic mirror and the meta-detector of the  
448 microscope. Bright-field images were acquired simultaneously using the transmission detector of  
449 the microscope. Fluorescence intensity was measured in 7  $\mu$ m ROI (Region Of Interest) at the root  
450 hair apex. For the lines SS-TOMATO and SS-TOMATO-EXT LONG in the different genetic  
451 backgrounds, roots were plasmolyzed with a 8% mannitol solution and the scanning was performed  
452 using Zeiss LSM 510 META (Zeiss, Germany)( Excitation: 543 nm argon laser; Emission: 560-600 nm,  
453 Zeiss Plain Apochromat 63X/1.4 -Oil objective). GFP signal and tdTOMATO cell wall signal at RH tip  
454 were quantified using the ImageJ software. Fluorescence AU were expressed as the mean  $\pm$  SD using  
455 the GraphPad Prism 8.0.1 (USA) statistical analysis software. Results are representative of two  
456 independent experiments, each involving 10 roots and approximately, between 10 to 20 hairs per  
457 root were observed.

458

459 **Peroxidase activity.** Soluble proteins were extracted from roots grown on agar plates in a Percival  
460 incubator at 22°C in a growth room for 10 days at 140  $\mu\text{mol m}^{-2}\text{s}^{-1}$  light intensity by grinding in  
461 20mM HEPES, pH 7.0, containing 1 mM EGTA, 10mM ascorbic acid, and PVP PolyclarAT (100mg  $\text{g}^{-1}$   
462 fresh material; Sigma, Buchs, Switzerland). The extract was centrifuged twice for 10 min at 10,000 g.  
463 Each extract was assayed for protein levels with the Bio-Rad assay (Bio-Rad). PRX activity was  
464 measured at 25°C by following the oxidation of 8 mM guaiacol (Fluka) at 470 nm in the presence of  
465 2 mM  $\text{H}_2\text{O}_2$  (Carlo Erba) in a phosphate buffer (200 mM, pH6.0). Values are the mean of three  
466 replicates  $\pm$  SD.

467  
468 **Cytoplasmic ROS (cytROS) measurements.** 2',7'-dichlorodihydrofluorescein diacetate ( $\text{H}_2\text{DCF-DA}$ ) is  
469 as a cell-permeable fluorogenic probe to quantify reactive oxygen species (ROS).  $\text{H}_2\text{DCFDA}$  diffuses  
470 into cells and is deacetylated by cellular esterases to form 2',7'-dichlorodihydrofluorescein ( $\text{H}_2\text{DCF}$ ).  
471 In the presence of ROS, predominantly  $\text{H}_2\text{O}_2$ ,  $\text{H}_2\text{DCF}$  is rapidly oxidized to 2',7'-dichlorofluorescein  
472 (DCF), which is highly fluorescent, with excitation and emission wavelengths of 498 and 522 nm,  
473 respectively. To measure cytoplasmic ROS in root hairs cells, growth of Arabidopsis seeds on a plate  
474 was done with 1% sterile agar for 8 d in a chamber at 22°C with continuous light. These seedlings  
475 were incubated in darkness on a slide for 10 min with 50  $\mu\text{M}$   $\text{H}_2\text{DCFDA}$  at room temperature.  
476 Samples were observed with Zeiss Imager A2 Epifluorescence. A 10 $\times$  objective was used, 0.30 N.A.,  
477 and exposure time 80-500ms. Images were analyzed using ImageJ 1.50b software. To measure ROS  
478 mean, a circular region of interest (ROI) ( $r=2.5$ ) was chosen in the tip zone of the root hair. All root  
479 hairs of six seedlings per genotype were analyzed. The reported values are the mean  $\pm$  standard  
480 deviation (mean  $\pm$  SD).

481  
482 **Apoplastic ROS ( $_{\text{apo}}$ ROS) measurements.** To measure apoplastic ROS in root hair cells, roots of 7-  
483 day-old seedlings were incubated with 50  $\mu\text{M}$  Amplex™ UltraRed Reagent (AUR, Molecular Probes)  
484 for 20 min in dark conditions and rinsed with liquid MS. Root hairs were imaged with a Zeiss LSM5  
485 Pascal laser scanning confocal microscope. The fluorescence emission of oxidized AUR in the  
486 apoplast of root hair cells was observed between 585 and 610 nm using 543 nm argon laser  
487 excitation, 40X objective, N/A=1.2. The intensity of fluorescence was quantified on digital images  
488 using ImageJ software. Quantification of the AUR probing fluorescence signal was restricted to  
489 apoplastic spaces at the root hair tip (as shown in **Figure 1**). The measurements were performed in  
490 three independent experiments ( $n = 6$ ) with the same microscopic settings.

491  
492 **Phylogenetic analysis.** 73 class-III PRX protein sequences from *A. thaliana*, two putative lignin class-  
493 III PRXs from *Zinnia elegans* and 4 putative Extensin class-III PRXs from *Lupinus album*, *Lycopersicum*  
494 *esculentum*, *Phaseolus vulgaris* and *Vitis vinifera*, have been aligned with ClustalW and the tree  
495 constructed using the Neighbor-Joining method (Saitou and Nei, 1987). The analyses were

496 conducted in MEGA7 (Kumar, 2016). All protein sequences are available using their ID number  
497 (<http://peroxibase.toulouse.inra.fr>) (Savelli et al., 2019).

498  
499 **Co-expression analysis network.** Co-expression networks for *RSL4* root hair genes were identified  
500 from PlaNet (<http://aranet.mpimp-golm.mpg.de>) and trimmed to facilitate readability (Mutwill et al.  
501 2011). Each co-expression of interest was confirmed independently using the expression angler tool  
502 from Botany Array Resource BAR ([http://bar.utoronto.ca/ntools/cgi-](http://bar.utoronto.ca/ntools/cgi-bin/ntools_expression_angler.cgi)  
503 [bin/ntools\\_expression\\_angler.cgi](http://bar.utoronto.ca/ntools/cgi-bin/ntools_expression_angler.cgi)) and ATTED-II (<http://atted.jp>). Only those genes that are  
504 connected with genes of interest are included.

505  
506 **Tyr-crosslinking analysis.** Alcohol-insoluble residues of root tissues obtained from *PRX01,44,73*  
507 mutants, Col-0 and 35Sp::PRX44-GFP lines were hydrolyzed in 6 N HCl (aqueous) with 10 mM phenol  
508 (2 mg ml<sup>-1</sup>; 110 °C; 20 h). Hydrolysates were dried under a steady stream of nitrogen (gas) and then  
509 re-dissolved at 10 mg ml<sup>-1</sup> in water. The hydrolysates were fractionated by gel permeation  
510 chromatography on a polyhydroxyethyl A column (inner diameter, 9.4 x 200 mm, 10 nm pore size,  
511 Poly LC Inc., Columbia, MD) equilibrated in 50 mM formic acid and eluted isocratically at a flow rate  
512 of 0.8 ml min<sup>-1</sup>. UV absorbance was monitored at 280 nm. The amounts of Tyr and IDT in the  
513 hydrolysates were then determined by comparison with peak areas of authentic Tyr and IDT  
514 standards. Response factors were determined from three level calibrations with the Tyr and IDT  
515 standards.

516  
517 **Immuno-blot Analysis.** Plant material (100 mg of root from 15 days old seedlings grown as indicated  
518 before) was collected in a microfuge tube and ground in liquid nitrogen with 400 µL of protein  
519 extraction buffer (125 mM Tris-Cl, pH. 4.4, 2% [w/v] SDS, 10% [v/v] glycerol, 6M UREA, 1% [v/v] b-  
520 mercaptoethanol, 1mM PMSF). Samples were immediately transferred to ice. After 4  
521 centrifugations at 13000 rpm for 20 min, supernatant was moved to a new 1.5 ml tube and equal  
522 volumes of Laemmli buffer (125 mM Tris-Cl, pH. 7.4, 4% [w/v] SDS, 40% [v/v] glycerol, 10% [v/v] β-  
523 mercaptoethanol, 0.002% [w/v] bromophenol blue) were added. The samples (0.5–1.0 mg/mL of  
524 protein) were boiled for 5 min and 30 µL were loaded on 10% SDS-PAGE. The proteins were  
525 separated by electrophoresis and transferred to nitrocellulose membranes. Anti-GFP mouse IgG  
526 (clones 7.1 and 13.1; Roche Applied Science) was used at a dilution of 1:2,000 and it was visualized  
527 by incubation with goat anti-mouse IgG secondary antibodies conjugated to horseradish peroxidase  
528 (1:2,000) followed by a chemiluminescence reaction (Clarity Western ECL Substrate; Bio-rad). For  
529 the SS-TOM lines analysis, proteins were extracted in 2x SDS buffer (4% SDS, 125mM Tris pH 6.8,  
530 20% glycerol, 0.01% bromophenol blue, 50 mM dithiothreitol [DTT]), using 10 µl of buffer per mg of  
531 plant tissues of Wt Col-0, transgenic lines 35S:SS-TOM and 35S:SS-TOM-Long-EXT. Two transgenic  
532 lines were analyzed. 10 µl of supernatant of each protein extract were run into a 12%  
533 polyacrylamide gel during one hour at 200 V, and then transferred to a PVDF membrane. PVDF was

534 blocked with 5% milk in TBST (Tris-HCl 10 mM, pH 7,4, NaCl 150 mM, Tween-20 at 0,05%) for 1 hour  
535 at 4°C and then washed four times during 15 min in TBST. An anti-RFP (A00682, GenScript) was used  
536 as primary antibody overnight at 4°C. Four washes of 15 min each in TBST at room temperature and  
537 then it was incubated two hours with a secondary antibody anti-rabbit (goat) conjugated with  
538 alkaline phosphatase (A3687, Sigma), in a 1:2,500 dilution with TBST. Four washes of 15 min each in  
539 TBST at room temperature. Finally, 10 ml of alkaline phosphatase (100mM Tris-HCl pH 9.5, 100 mM  
540 NaCl, 3 mM MgCl<sub>2</sub>) containing 80 µl NBT (Sigma) (35mg/ml in 70% DMSO and 30 µl de BCIP (Sigma)  
541 (50 mg/ml in 100% de DMSO) were used.

542  
543 **Transmission electron microscopy of root hair cell walls.** Seeds were germinated on 0.2x MS, 1%  
544 sucrose, 0.8% agar. Seven days after germination, seedlings were transferred to new 0.2x MS, 1%  
545 sucrose, 0.8% agar plates with or without 100 µM SHAM. After 4 additional days, 1-mm root  
546 segments with root hairs were fixed in 2% glutaraldehyde in 0.1M cacodylate buffer pH7.4. Samples  
547 were rinsed in cacodylate buffer and post-fixed in 2% OsO<sub>4</sub>. After dehydration in ethanol and  
548 acetone, samples were infiltrated in Epon resin (Ted Pella, Redding, CA). Polymerization was  
549 performed at 60°C. Sections were stained with 2% uranyl acetate in 70% methanol followed by  
550 Reynold's lead citrate (2.6% lead nitrate and 3.5% sodium citrate [pH 12.0]) and observed in a Tecnai  
551 12 electron microscope. Quantitative analysis of cell wall thickness was performed using FIJI.

552  
553 **Modeling and molecular docking between PRXs and EXTs.** Modeling and molecular docking: cDNA  
554 sequences of PRXs were retrieved from TAIR (PRX01: AT1G05240, PRX36: AT3G50990, PRX44:  
555 AT4G26010, PRX64: AT5G42180, PRX73: AT5G67400) and NCBI Nucleotide DB (PRX24Gv:Vitis  
556 vinifera peroxidase 24, GvEP1, LOC100254434). Homology modeling was performed for all PRXs  
557 using modeller 9.14 (Sali et al. 1993), using the crystal structures 1PA2, 3HDL, 1QO4 and 1HCH as  
558 templates, available at the protein data bank. 100 structures were generated for each protein and  
559 the best scoring one (according to DOPE score) was picked. The *receptor* for the docking runs was  
560 generated by the prepare\_receptor4 script from autodock suite, adding hydrogens and constructing  
561 bonds. Peptides based on the sequence PYSPSPKVVYPPSSVYPPPPS were used, replacing proline  
562 by hydroxyproline, and/or adding O-Hyp glycosylation with up to four arabinoses per hydroxyproline  
563 in the fully glycosylated peptide and a galactose on the serine, as it is usual in plant O-Hyp  
564 <https://www.ncbi.nlm.nih.gov/pmc/articles/PMC5045529/>. Ligand starting structure was generated  
565 as the most stable structure by molecular dynamics (Velasquez et al. 2015a). All ligand bonds were  
566 set to be able to rotate. Docking was performed in two steps, using Autodock vina (Trott et al.  
567 2010). First, an exploratory search over the whole protein surface (exhaustiveness 4) was done,  
568 followed by a more exhaustive one (exhaustiveness 8), reducing the search space to a 75x75x75 box  
569 centered over the most frequent binding site found in the former run.

570

571 **EXT conformational coarse-grained model.** The use of coarse-grained (CG) molecular dynamics  
572 (MD) allowed collection of long timescale trajectories. System reduction is significant when  
573 compared to all atom models, approximately reducing on order of magnitude in particle number. In  
574 addition, a longer integration time step can be used. Protein residues and coarse grained solvent  
575 parameters correspond to the SIRAH model (Darré et al. 2015), while ad hoc specific glycan  
576 parameters were developed. The CG force field parameters developed correspond to  
577 arabinofuranose and galactopyranose (**Figure S5**). Triple helix systems were simulated both, in the  
578 non-glycosylated and fully *O*-glycosylated states, where all the hydroxyprolines are bound to a  
579 tetrasaccharide of arabinofuranoses, and specific serine residues contain one galactopyranose  
580 molecule. They were immersed in WT4 GC solvent box that was constructed to be 2 nm apart from  
581 the extensin fiber, and periodic boundary conditions were employed. Coarse grained ions were also  
582 included to achieve electroneutrality and 0.15 M ionic strength. All simulations were performed  
583 using the GROMACS MD package at constant temperature and pressure, using the Berendsen  
584 thermostat (respectively) and Parrinello-Rahman barostat (Parrinello and Rahman 1981), and a 10 fs  
585 time step. The obtained trajectories were analysed using the Mdtraj python package (McGibbon et  
586 al, 2015) and visualized with Visual Molecular Dynamics (VMD) 1.9.1 (Humphrey et al. 1996).  
587 Volume measurements were performed using a Convex Hull algorithm implemented in NumPy  
588 (Oliphant 2006), and average diameter calculations were derived from this quantity using simple  
589 geometric arguments.

590

591 **Acknowledgements**

592 We thank Andres Rossi from the microscopy facility of FIL for his assistance. We thank ABRC (Ohio  
593 State University) for providing T-DNA lines seed lines. J.M.E. is Principal Investigator of the National  
594 Research Council (CONICET) from Argentina. This work was supported by grants from ANPCyT  
595 (PICT2017-0066, and PICT2019-0015), by ANID – Programa Iniciativa Científica Milenio ICN17\_022,  
596 NCN2021\_010 and Fondo Nacional de Desarrollo Científico y Tecnológico [1200010] to J.M.E, from  
597 ANPCyT (PICT2018-00577) to E.M., and NSF MCB grant 1614965 to M.S.O.

598

599 **Author Contribution**

600 E.M and C.B performed most of the experiments and analysed the data. P.R. and C.D. analysed the  
601 peroxidase activity and performed phylogenetic analysis. J.W.M-E and M.H. analysed the Tyr-  
602 crosslinking on EXTs. A.A.A. and A.D.N performed the docking experiments and analysed this data.  
603 M.B. and L.C. perform the EXT modelling and analysed this data. M.F. and P.B generated the EXT  
604 reporter lines and performed the immune-blots analysis of SS-TOM and SS-TOM-Long-EXT lines.  
605 J.M.P., D.R.R.G., Y.d.C.R.G., S.M., J.M.P. and F.B.H. analysed the data. J.P., J.P-V., and M.S.O.  
606 performed the transmission electron microscopy analysis. J.M.E. designed research, analysed the  
607 data, supervised the project, and wrote the paper. All authors commented on the results and the  
608 manuscript. This manuscript has not been published and is not under consideration for publication  
609 elsewhere. All the authors have read the manuscript and have approved this submission.

610

611 **Competing financial interest**

612 The authors declare no competing financial interests. Correspondence and requests for materials  
613 should be addressed to J.M.E. (Email: [jestevez@leloir.org.ar](mailto:jestevez@leloir.org.ar)).

614

615 **REFERENCES**

- 616 Baumberger N, Ringli C, Keller B. (2001). The chimeric leucine rich repeat/extensin cell wall protein  
617 LRX1 is required for root hair morphogenesis in *Arabidopsis thaliana*. *Genes & Development* 15,  
618 1128–1139.
- 619 Baumberger N, Steiner M, Ryser U, Keller B, Ringli C. (2003). Synergistic interaction of the two  
620 paralogous Arabidopsis genes LRX1 and LRX2 in cell wall formation during root hair  
621 development. *Plant J.* 35, 71–81.
- 622 Berendsen, H. J. C., Postma, J.P.M., van Gunsteren, W.F., DiNola, A., and Haak, J.R. (1984) Molecular  
623 dynamics with coupling to an external bath. *J. Chem. Phys.* 81, 3684. doi: 10.1063/1.448118.
- 624 Berman HM, John Westbrook, Zukang Feng, Gary Gilliland, Talapady N Bhat, Helge Weissig, Ilya N  
625 Shindyalov, and Philip E Bourne. The protein data bank. *Nucleic Acids Research*, 28(1):235–242,  
626 2000.
- 627 Bernards, M.A., Fleming, W.D., Llewellyn, D.B., Priefer, R., Yang, X., Sabatino, A., and Plourde, G.L.  
628 (1999). Biochemical characterization of the suberization-associated anionic peroxidase of  
629 potato. *Plant Physiol.* 121: 135–146.
- 630 Bhavé G, Cummings CF, Vanacore RM, Kumagai-Cresse C, Ero-Tolliver IA, Rafi M, Kang J-S,  
631 Pedchenko V, Fessler LI, Fessler JH, Hudson BG (2012) Peroxidasin forms sulfilimine chemical  
632 bonds using hypohalous acids in tissue genesis. *Nat. Chem. Biol.* 8:784–790.
- 633 Brady, J.D., Sadler, I.H., and Fry, S.C. (1996). Di-isodityrosine, a novel tetrameric derivative of  
634 tyrosine in plant cell wall proteins: a new potential cross-link. *Biochem. J* 315: 323–327.
- 635 Brady, J.D., Sadler, I.H., and Fry, S.C. (1998). Pulcherosine, an oxidatively coupled trimer of tyrosine  
636 in plant cell walls: its role in cross-link formation. *Phytochemistry.* 47(3):349-353.
- 637 Brown K.L, C.F. Cummings, R.M. Vanacore and B.G. Hudson. (2017). Building collagen IV smart  
638 scaffolds on the outside of cells. *Protein Sci.* 26:2151-2161.
- 639 Brownleader, M.D., Ahmed, N., Trevan, M., Chaplin, M.F., and Dey, P.M. (1995). Purification and  
640 partial characterization of Tomato extensin peroxidase. *Plant Physiol.* 109: 1115–1123
- 641 Cannon, M.C., Terneus, K., Hall, Q., Tan, L., Wang, Y., Wegenhart, B.L., Chen, L., Lamport, D.T., Chen,  
642 Y., and Kieliszewski, M.J. (2008). Self-assembly of the plant cell wall requires an extensin  
643 scaffold. *Proc. Natl. Acad. Sci. USA.* 105: 2226–2231.
- 644 Chen, Y., Dong, W., Tan, L., Held, M. A., & Kieliszewski, M. J. (2015). Arabinosylation plays a crucial  
645 role in extensin cross-linking in vitro. *Biochemistry insights*, 8, BCI-S31353.
- 646 Cosio C. & Dunand C. (2009). Specific functions of individual class III peroxidases genes. *J. Exp. Bot.*  
647 62:391–408.
- 648 Cosio C., Ranocha Ph., Francoz E., Burlat V., Zheng Y., Perry S.E., Ripoll J.-J., Yanofsky M., Dunand C.  
649 (2017) The class III peroxidase PRX17 is a direct target of the MADS-box transcription factor 1  
650 AGL15 and participates in lignified tissue formation. *New Phytol.* 213: 250-263.
- 651 Darré, L., Machado, M.R., Brandner, A.F., González, H.C., Ferreira, S., and Pantano, S. (2015). SIRAH:  
652 A structurally unbiased coarse-grained force field for proteins with aqueous solvation and long-  
653 range electrostatics. *J. Chem. Theory Comput.* 11(2):723–739.
- 654 Davey, C. A. and R. E. Fenna (1996). 2.3 Å resolution X-ray crystal structure of the bisubstrate  
655 analogue inhibitor salicylhydroxamic acid bound to human myeloperoxidase: a model for a  
656 prereaction complex with hydrogen peroxide. *Biochemistry* 35(33): 10967-10973.

657 Dong, W., Kieliszewski, M., and Held, M.A. (2015). Identification of the pI 4.6 extensin peroxidase  
658 from *Lycopersicon esculentum* using proteomics and reverse-genomics. *Phytochem.* 112:151–  
659 159.

660 Dunand, C., Crevecoeur, M., and Penel, C. (2007). Distribution of superoxide and hydrogen peroxide  
661 in Arabidopsis root and their influence on root development: possible interaction with  
662 peroxidases. *New Phytol.* 174:332–341.

663 Dynowski M, Schaaf G, Loque D, Moran O, Ludewig U (2008) Plant plasma membrane water  
664 channels conduct the signalling molecule H<sub>2</sub>O<sub>2</sub>. *Biochem J* 414: 53–56.

665 Egelund, J., Obel, N., Ulvskov, P., Geshi, N., Pauly, M., Bacic, A., and Larsen Petersen, B. (2007).  
666 Molecular characterization of two Arabidopsis thaliana glycosyltransferase mutants, rra1 and  
667 rra2, which have a reduced residual arabinose content in a polymer tightly associated with the  
668 cellulosic wall residue. *Plant. Mol. Biol.* 64:439–451.

669 Fabrice T, Vogler H, Draeger C, Munglani G, Gupta S, Herger A, Knox P, Grossniklaus U, Ringli C.  
670 (2018). LRX Proteins play a crucial role in pollen grain and pollen tube cell wall development.  
671 *Plant Physiology* 176: 1981–1992.

672 Francoz et al. (2019) Pectin demethylesterification generates platforms that anchor peroxidases to  
673 remodel plant cell wall domains. *Developmental Cell* 48, 1-16.

674 Hall, Q., and Cannon, M.C. (2002). The cell wall hydroxyproline-rich glycoprotein RSH is essential for  
675 normal embryo development in Arabidopsis. *Plant Cell* 14: 1161–1172.

676 Held, M. A., Tan, L., Kamyab, A., Hare, M., Shpak, E., and Kieliszewski, M. J. (2004). Di-isodityrosine is  
677 the intermolecular cross-link of isodityrosine-rich extensin analogs cross-linked in vitro. *Journal*  
678 *of Biological Chemistry*, 279(53), 55474-55482.

679 Herrero, J., Fernández-Pérez, F., Yebra, T., Novo-Uzal, E., Pomar, F., Pedreño, M.Á., Cuello, J., Guéra,  
680 A., Esteban-Carrasco, A., and Zapata, J.M. (2013). Bioinformatic and functional characterization  
681 of the basic peroxidase 72 from Arabidopsis thaliana involved in lignin biosynthesis. *Planta* 237:  
682 1599–1612.

683 Hooijmaijers C, Rhee JY, Kwak KJ, Chung GC, Horie T, Katsuhara M, Kang H (2012) Hydrogen peroxide  
684 permeability of plasma membrane aquaporins of *Arabidopsis thaliana*. *J Plant Res* 125: 147–153.

685 Humphrey, W., Dalke, A., and Schulten, K. (1996). VMD: Visual molecular dynamics. *J. Molec.*  
686 *Graphics* 14:33-38

687 Ikeda-Saito, M., D. A. Shelley, L. Lu, K. Booth, W. Caughey and S. Kimura (1991). Salicylhydroxamic  
688 acid inhibits myeloperoxidase activity. *Journal of Biological Chemistry* 266(6): 3611-3616

689 Ishiwata A, Kaeothip S, Takeda Y, Ito Y (2014) Synthesis of the highly glycosylated hydrophilic motif  
690 of extensins. *Angew Chem Int Ed Engl* 53: 9812–9816

691 Jackson, P.A., Galinha, C.I., Pereira, C.S., Fortunato, A., Soares, N.C., Amâncio, S.B., and Pinto  
692 Ricardo, C.P. (2001). Rapid deposition of extensin during the elicitation of grapevine callus  
693 cultures is specifically catalyzed by a 40-kilodalton peroxidase. *Plant Physiol.* 127: 1065–1076.

694 Jacobowitz, J.R, Doyle W.C., and Weng, J-K. (2019). PRX9 and PRX40 are extensin peroxidases  
695 essential for maintaining tapetum and microspore cell wall integrity during Arabidopsis anther  
696 development. *Plant Cell* 31: 848–86.

697 Kim D Pruitt, Tatiana Tatusova, and Donna R Maglott. Ncbi reference sequences (refseq): a curated  
698 non-redundant sequence database of genomes, transcripts and proteins. *Nucleic Acids Research*,  
699 35(suppl 1):D61–D65, 2006.

700 Kumar, S., Stecher G., Tamura K. (2016) MEGA7: molecular evolutionary genetic analysis version 7.0  
701 for bigger datasets. *Mol. Biol. Evol.* 33(7): 1870-1874.

702 Kunieda, T., Shimada, T., Kondo, M., Nishimura, M., Nishitani, K., and Hara-Nishimura, I. (2013).  
703 Spatiotemporal secretion of PEROXIDASE36 is required for seed coat mucilage extrusion in  
704 *Arabidopsis*. *Plant Cell* 25: 1355–1367.

705 Lamport, D.T.A., Kieliszewski, M.J., Chen, Y., and Cannon, M.C. (2011). Role of the extensin  
706 superfamily in primary cell wall architecture. *Plant Physiol.* 156: 11–19.

707 Lee, Y., Rubio, M.C., Alassimone, J., and Geldner, N. (2013). A mechanism for localized lignin  
708 deposition in the endodermis. *Cell* 153: 402–412.

709 Mangano S. *et al.* (2017). The molecular link between auxin and ROS-controlled root hair growth.  
710 *Proc. Natl. Acad. Sci. U.S.A.* 114(20):5289-5294.

711 Martinez Pacheco J *et al.* (2022). Apoplastic class III peroxidases PRX62 and PRX69 promote  
712 *Arabidopsis* root hair growth at low temperature. *BioRxiv* doi.org/10.1101/2021.08.20.456256.

713 Martin Emily R. *et al.* (2022). Ethylene signaling increases reactive oxygen species accumulation to  
714 drive root hair initiation in *Arabidopsis*. *BioRxiv* doi.org/10.1101/2021.11.14.468514.

715 Marzol E, Borassi C, Bringas M, Sede A, Rodríguez Garcia DR, Capece L, Estevez JM. (2018). Filling the  
716 Gaps to Solve the Extensin Puzzle. *Mol Plant.* 11(5):645-658.

717 McGibbon R.T, Beauchamp K.A., Harrigan M.P., Klein C., Swails, J.M., Hernández C.X., Schwantes  
718 C.R., Wang, L.P., Lane T.J., Pande V.S. (2015) MDTraj: A Modern Open Library for the Analysis of  
719 Molecular Dynamics Trajectories. *Biophysical Journal*, 109(8): 1528-1532.

720 Møller, S.R., et al. (2017). Identification and evolution of a plant cell wall specific glycoprotein  
721 glycosyl transferase, ExAD. *Sci. Rep.* 7: 45341.

722 Monshausen GB, Bibikova TN, Messerli MA, Shi C, Gilroy S (2007) Oscillations in extracellular pH and  
723 reactive oxygen species modulate tip growth of *Arabidopsis* root hairs. *Proc Natl Acad Sci USA*  
724 104:20996–21001.

725 Mutwil, M., Klie, S., Tohge, T., Giorgi, F.M., Wilkins, O., Campbell, M.M., Fernie, A.R., Usadel, B.,  
726 Nikoloski, Z. and Persson, S. (2011). PlaNet: combined sequence and expression comparisons  
727 across plant networks derived from seven species. *Plant Cell*, 23, 895– 910.

728 Oliphant, TE. USA: Trelgol Publishing, (2006). A guide to NumPy. 376 pp.

729 Orman-Ligeza B, et al. (2016) RBOH-mediated ROS production facilitates lateral root emergence in  
730 *Arabidopsis*. *Development* 143:3328–3339

731 Owens NW, Stetefeld J, Lattová E, Schweizer F (2010) Contiguous *O*-galactosylation of 4(R)-hydroxy-  
732 l-proline residues forms very stable polyproline II helices. *J Am Chem Soc* 132: 5036–5042

733 Parrinello, M. and Rahman, A. (1981). Polymorphic transitions in single crystals: A new molecular  
734 dynamics method. *J. of Applied Physics* 52:7182. doi.org/10.1063/1.328693

735 Passardi, F., Penel, C., and Dunand, C. (2004). Performing the paradoxical: how plant peroxidases  
736 modify the cell wall. *Trends Plant Sci.* 9:534–540.

737 Pereira S.P., J.M.L. Ribeiro, A.D. Vatulescu, K. Findlay, A.J. MacDougall and P.A.P. Jackson. (2011)  
738 Extensin network formation in *Vitis vinifera* callus cells is an essential and causal event in rapid  
739 and H<sub>2</sub>O<sub>2</sub>-induced reduction in primary cell wall hydration. *BMC Plant Biology* 11:106-121.

740 Pereira Graças, J et al. (2022) Ethylene signaling causing tolerance of *Arabidopsis thaliana* roots to  
741 low pH stress is linked to class III peroxidase activity. *Journal of Plant Growth Regulation* 40, 116–  
742 125.

743 Price, N.J., Pinheiro, C., Soares, C.M., Ashford, D.A., Ricardo, C.P., and Jackson, P.A. (2003). A  
744 biochemical and molecular characterization of LEP1, an extensin peroxidase from lupin. *J. Biol.*  
745 *Chem.* 278:41389–41399.

746 Ringli C. (2010). The hydroxyproline-rich glycoprotein domain of the Arabidopsis LRX1 requires Tyr  
747 for function but not for insolubilization in the cell wall. *Plant J.* 63, 662–669.

748 Rodrigues, O. et al. (2017). Aquaporins facilitate hydrogen peroxide entry into guard cells to mediate  
749 ABA- and pathogen-triggered stomatal closure. *Proc Natl Acad Sci USA* 114, 9200–9205,  
750 doi:10.1073/pnas.1704754114.

751 Saito, F., Suyama, A., Oka, T., Yoko-o, T., Matsuoka, K., Jigami, Y., and Shimma, Y. (2014).  
752 Identification of novel peptidyl serine O-galactosyltransferase gene family in plants. *J. Biol.*  
753 *Chem.* 30:20405–20420.

754 Saitou N, Nei M. (1987). The neighbor-joining method: a new method for reconstruction of  
755 phylogenetic trees. *Mol Biol Evol*4:406–25.

756 Šali A., and Tom L Blundell. (1993). Comparative protein modelling by satisfaction of spatial  
757 restraints. *J. of Molecular biology*, 234(3):779–815.

758 Savelli B., Li Q., Webber M., Jemmat A.M., Robitaille A., Zamocky M., Mathe C., Dunand C. (2019).  
759 RedoxiBase a database for ROS homeostasis regulated proteins. *Redox Biol.*  
760 doi.org/10.1016/j.redox.2019.101247.

761 Schnabelrauch, L.S., Kieliszewski, M., Upham, B.L., Alizedeh, H., and Lamport, D. (1996). Isolation of  
762 pl 4.6 extensin peroxidase from tomato cell suspension cultures and identification of Val-Tyr-Lys  
763 as putative intermolecular cross-link site. *Plant J.* 9:477–489.

764 Sede, A.R., Borassi, C., Wengier, D.L., Mecchia, M.A., Estevez, J.M., and Muschietti, J.P. (2018).  
765 Arabidopsis pollen extensins LRX are required for cell wall integrity during pollen tube growth.  
766 *FEBS Lett.* 592, 233–243.

767 Shen Y., Rosendale M., Campbell R.E., D. Perrais (2014). pHuji, a pH-sensitive red fluorescent protein  
768 for imaging of exo- and endocytosis. *J. Cell Biol.* 207 (3):419–432.

769 Smith, A.T., Santama, N., Dacey, S., Edwards, M., Bray, R.C., Thorneley, R.N., and Burke, J.F. (1990).  
770 Expression of a synthetic gene for horseradish peroxidase C in *Escherichia coli* and folding and  
771 activation of the recombinant enzyme with Ca<sup>2+</sup> and heme. *J. Biol. Chem.* 265: 13335–13343.

772 Stafstrom, J.P., and Staehelin, L.A. (1986). The role of carbohydrate in maintaining extensin in an  
773 extended conformation. *Plant Physiol.* 81:242–246.

774 Stoddard, A and Rolland, V. (2018). I see the light!. Fluorescent proteins suitable for the cell  
775 wall/apoplast targeting in *Nicotiana benthamiana* leaves. *Plant Direct.* doi.org/10.1002/pld3.112

776 Strasser, R. (2016). Plant protein glycosylation. *Glycobiology.* 26(9):926–939.

777 Stratford, S., et al. (2001). A leucine-rich repeat region is conserved in pollen extensin-like (Pex)  
778 proteins in monocots and dicots. *Plant Mol. Biol.* 46:43–56.

779 Takeda S, et al. (2008) Local positive feedback regulation determines cell shape in root hair cells.  
780 *Science* 319:1241–1244.

781 Trott O., and Arthur J Olson. (2010). Autodock vina: improving the speed and accuracy of docking  
782 with a new scoring function, efficient optimization, and multithreading. *Journal of*  
783 *Computational Chem.* 31(2):455–461.

784 Vanacore R, Ham AJ, Voehler M, Sanders CR, Conrads TP, Veenstra TD, Sharpless KB, Dawson PE,  
785 Hudson BG (2009) A sulfilimine bond identified in collagen IV. *Science* 325:1230–1234.

786 Velasquez, S.M., Ricardi, M.M., Dorosz, J.G., Fernandez, P.V., Nadra, A.D., Pol-Fachin, L., Egelund, J.,  
787 Gille, S., Ciancia, M., Verli, H., et al. (2011). O-glycosylated cell wall extensins are essential in root  
788 hair growth. *Science* 332:1401–1403.

789 Velasquez M, Salter JS, Dorosz JG, Petersen BL, Estevez JM. (2012). Recent advances on the  
790 posttranslational modifications of EXTs and their roles in plant cell walls. *Frontiers in plant*  
791 *science* 3, 93.

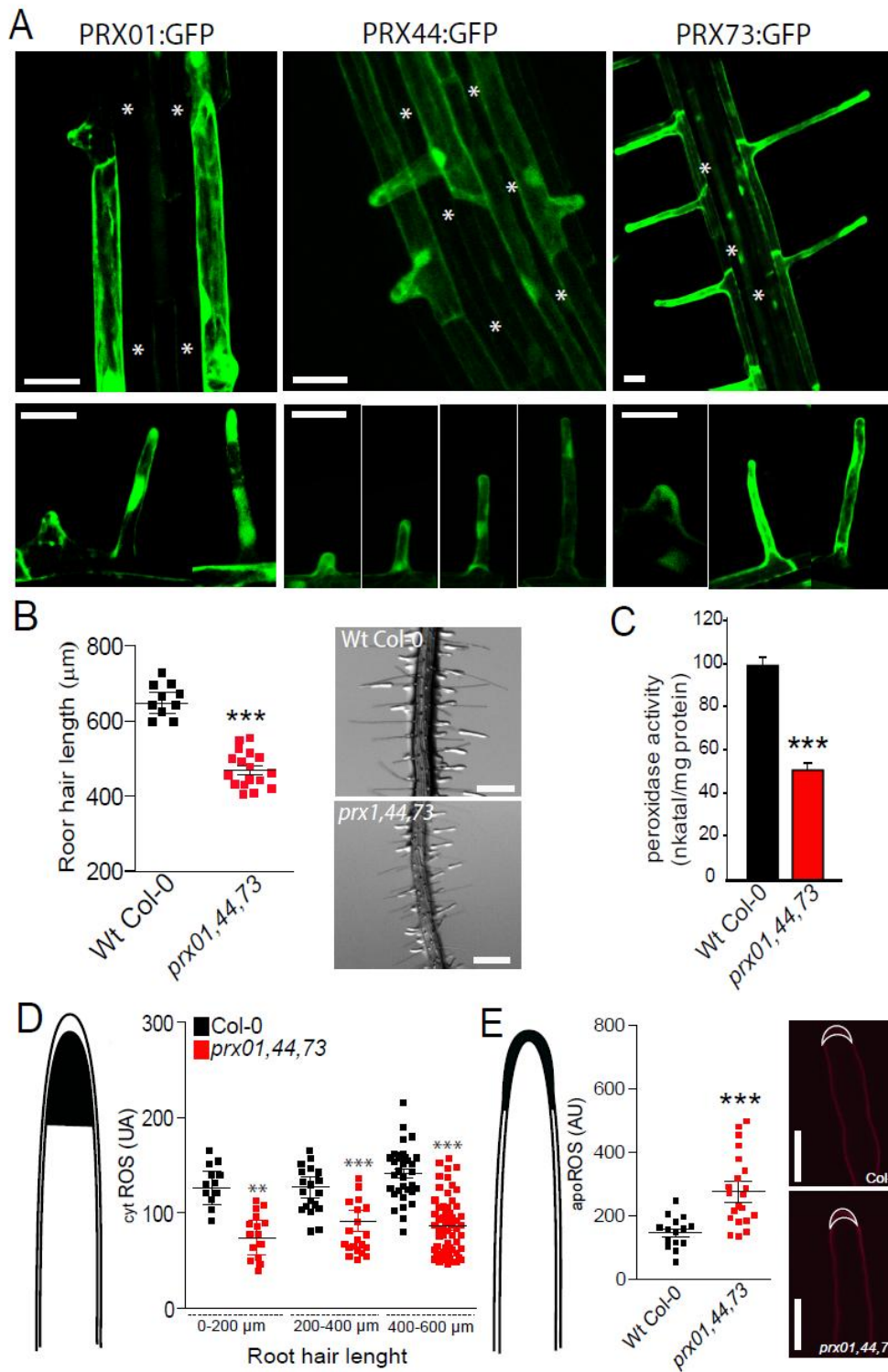
792 Velasquez SM, Marzol E, Borassi C, Pol-Fachin L, Ricardi MM, Mangano S, Denita JS, Salgado SJ,  
793 Gloazzo DJ, Marcus SE. (2015a). Low sugar is not always good: Impact of specific O-glycan  
794 defects on tip growth in Arabidopsis. *Plant Physiology* 168, 808–813.

795 Velasquez, S.M., Ricardi, M.M., Poulsen, C.P., Oikawa, A., Dilokpimol, A., Halim, A., Mangano, S.,  
796 Denita-Juarez, S.P., Marzol, E., Salgoda Salter, J.D., et al. (2015b). Complex regulation of prolyl-4-  
797 hydroxylases impacts root hair expansion. *Mol. Plant* 8:734–746.

798 Wang, X., Wang, K., Yin, G., Liu, X., Liu, M., Cao, N., Duan, Y., Gao, H., Wang, W., Ge, W., et al.  
799 (2018). Pollen-expressed leucine-rich repeat extensins are essential for pollen germination and  
800 growth. *Plant Physiol.* 176, 1993–2006.

801 Wojtaszek, P., Trethowan, J., and Bolwell, G.P. (1997). Reconstitution in vitro of the components and  
802 conditions required for the oxidative cross-linking of extracellular proteins in French bean  
803 (*Phaseolus vulgaris* L.). *FEBS Lett.* 405:95–98.

804 Yi K, Menand B, Bell E, Dolan L. (2010). A basic helix-loop-helix transcription factor controls cell  
805 growth and size in root hairs. *Nature genetics* 43: 264-267.



809 **Figure 1. Characterization of root hair-specific PRX01, PRX44 and PRX73 expression and mutant**  
810 **analysis.**

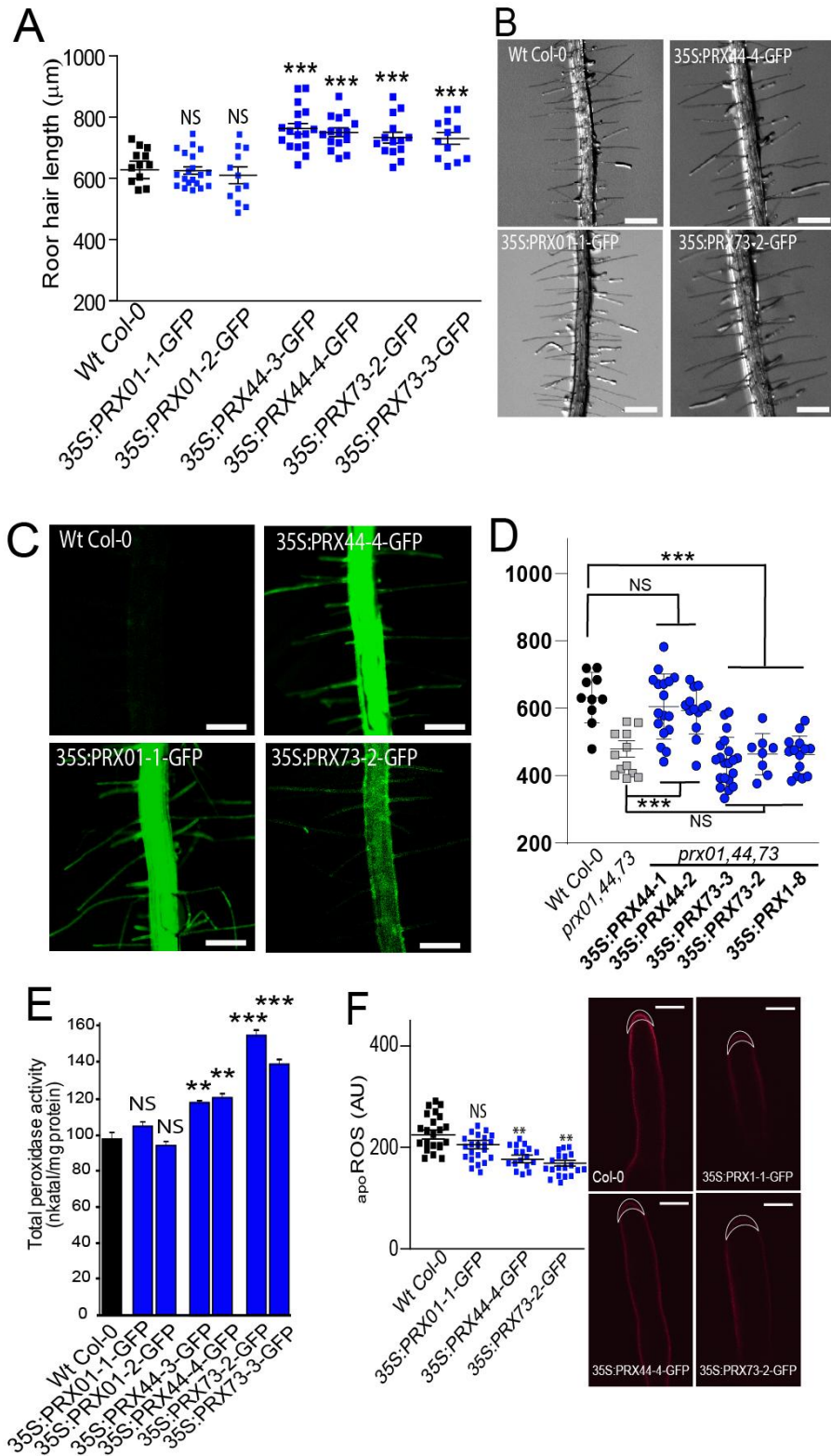
811 (A) GFP-tagged transcriptional reporters of PRX01, PRX44 and PRX73 show expression in the root  
812 elongation zone and specifically in root hairs (bottom). Scale bar = 20  $\mu$ m. (\*) indicates atrichoblast  
813 cell layers, which lack GFP expression.

814 (B) Root hair length phenotype of Wt and the *prx01,44,73* triple mutant. Left, box-plot of root hair  
815 length. Horizontal lines show the means. P-value determined by one-way ANOVA, (\*\*\*)  $P < 0.001$ .  
816 Right, bright-field images exemplifying the root hair phenotype in each genotype. Scale bars, 1 mm.

817 (C) Peroxidase activity in Wt and *prx01,44,73* triple mutant roots. Enzyme activity values (expressed  
818 as nkatal/mg protein) are shown as the mean of three replicates  $\pm$  SD. P-value determined by one-  
819 way ANOVA, (\*\*\*)  $P < 0.001$ .

820 (D) Cytoplasmic ROS levels measured with H<sub>2</sub>DCF-DA in Wt and *prx01,44,73* triple mutant root hairs.  
821 Horizontal lines show the means. P-values determined by one-way ANOVA, (\*\*\*)  $P < 0.001$  and (\*\*)  
822  $P < 0.01$ .

823 (E) Apoplastic ROS levels measured with Amplex™ UltraRed (AUR) in Wt and *prx01,44,73* triple  
824 mutant root hairs. ROS signal was quantified from the root hair cell tip. Left, box-plot of apoROS  
825 values. Horizontal lines show the means. P-value determined by one-way ANOVA, (\*\*\*)  $P < 0.001$ .  
826 Right, fluorescence images exemplifying apoROS detection in root hair apoplast.



830 **Figure 2. Partially redundant functions of PRX01, PRX44 and PRX73 in promoting root hair growth**  
831 **linked to their peroxidase activity.**

832 (A) Root hair length phenotype of Wt and PRX<sup>OE</sup> lines (in Wt background). Box-plot of root hair  
833 length. Horizontal lines show the means. P-values determined by one-way ANOVA, (\*\*\*) P<0.001,  
834 (NS) not significantly different.

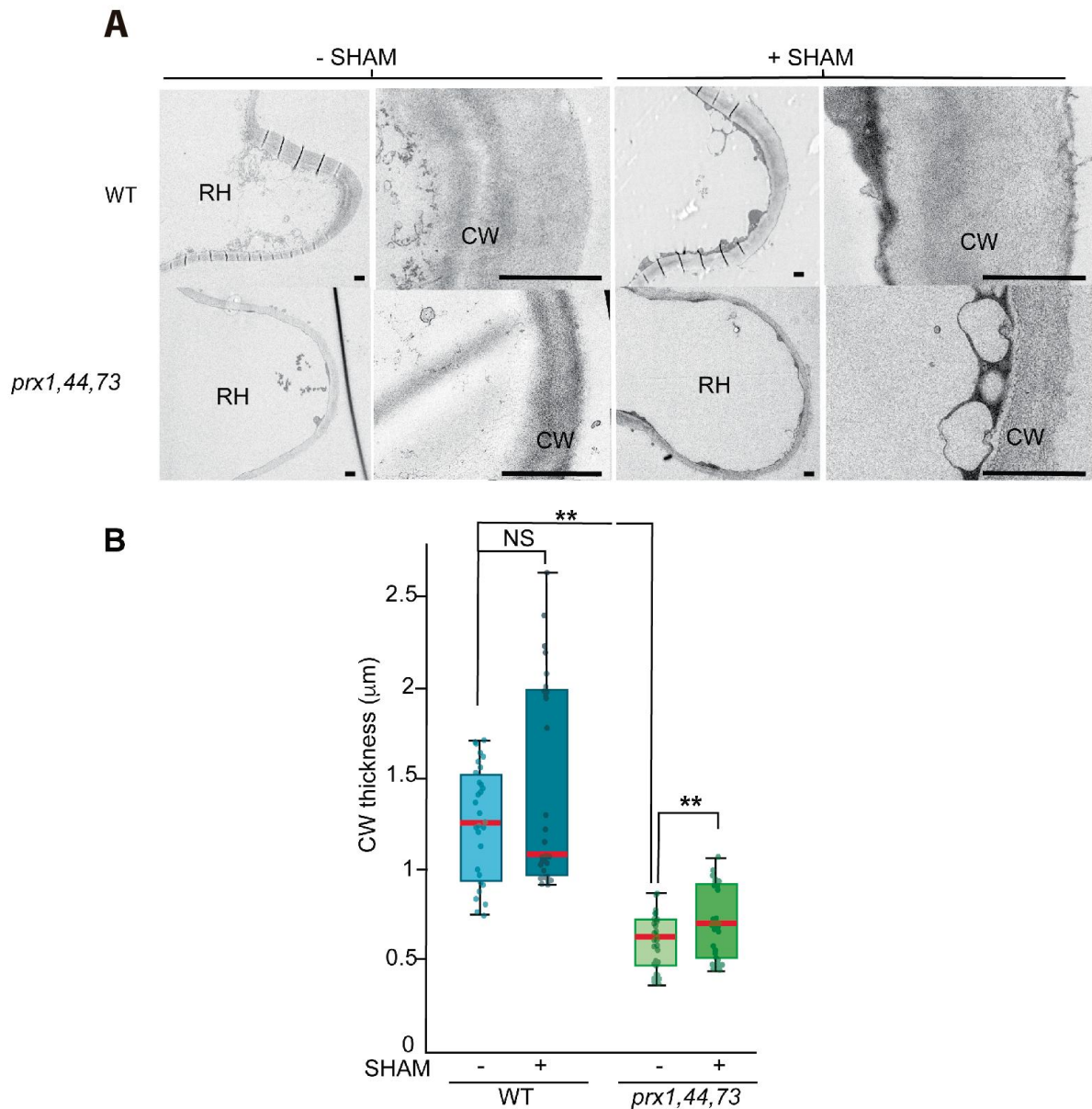
835 (B) Bright-field images exemplifying the root hair phenotype analyzed in Figure 2A. Scale bar = 0.5  
836 mm.

837 (C) Expression of GFP-tagged 35S:PRX01, 35S:PRX44 and 35S:PRX73 in root hair cells.

838 (D) Root hair length phenotype of Wt, *prx01,44,73* triple mutant and PRX<sup>OE</sup> lines (in *prx01,44,73*  
839 triple mutant background). Left, box-plot of root hair length. Horizontal lines show the means. P-  
840 value determined by one-way ANOVA, (\*\*\*) P<0.001.

841 (E) Assays of total peroxidase activity in Wt and PRXs<sup>OE</sup> lines (in Wt background). Enzyme activity  
842 (expressed in nkatal/mg protein) was determined by a guaiacol oxidation-based assay. Values are  
843 the mean of three replicates ± SD. P-values determined by one-way ANOVA, (\*\*\*) P<0.001, (\*\*)  
844 P<0.01, (NS) not significantly different.

845 (F) Apoplastic ROS levels measured with Amplex™ UltraRed (AUR) in Wt and PRX<sup>OE</sup> lines (in Wt  
846 background). ROS signal was quantified from the root hair cell tip. Left, box plot of apoROS values.  
847 Horizontal lines show the means. P-values determined by one-way ANOVA, (\*\*) P<0.01, (NS) not  
848 significantly different. Right, fluorescence images exemplifying apoROS detection in root hair  
849 apoplast. Scale bar = 10 μm.

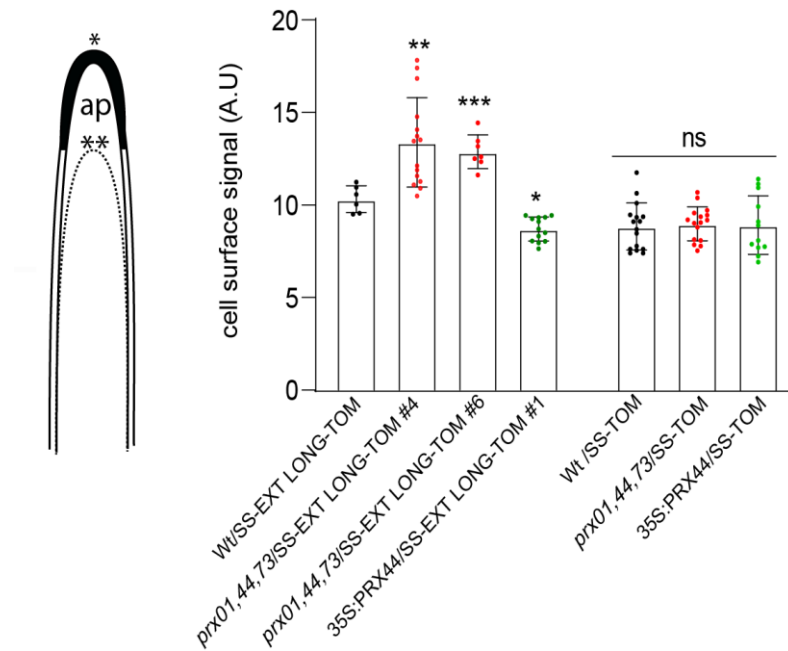


851

852 **Figure 3. Effect of PRX expression on cell wall thickness in root hair tips.**

853 (A) Transmission electron micrographs of root hair tips from Wt, *prx01,44,73* triple mutant, and  
 854 PRX44<sup>OE</sup> with (+) and without (-) peroxidase inhibitor SHAM. For each genotype and treatment, a  
 855 representative overview of a root hair (RH) and a detail of the cell wall at the root hair tip (CW) is  
 856 shown. Scale bar = 1 μm.

857 (B) Box and whisker plot showing cell wall thickness measured at the root hair tip of the three  
858 genotypes with or without SHAM treatment. (\*\*)  $P < 0.001$  determined by t-test. (NS) not  
859 significantly different.



861

862

863 **Figure 4. EXT-stabilization in RH apical cell wall depends on PRX01, PRX44, PRX73.** Signal of SS-  
 864 TOM and SS-EXT LONG-TOM in the apical zone of RHs in Col-0, in the triple mutant *prx01,44,73*, and  
 865 in 35S:PRX44. Cells were plasmolyzed with mannitol 8%. In the images: (\*) indicates cell surface  
 866 including the plant cell walls, (\*\*) indicates the retraction of the plasma membrane, (ap) apoplastic  
 867 space delimited between the plant cell wall and the retracted plasma membrane. Each point is the  
 868 signal derived from a single RH tip. Fluorescence AU data are the mean  $\pm$  SD (N=10 root hairs), two-  
 869 way ANOVA followed by a Tukey–Kramer test; (\*)  $p < 0.05$ , (\*\*)  $p < 0.01$ , (\*\*\*)  $p < 0.001$ . Results are  
 870 representative of two independent experiments. Asterisks on the graph indicate significant  
 871 differences between genotypes. NS= non-significant differences.

872  
873  
874  
875  
876  
877

**Table 1.** Peptidyl-Tyr and iso-dityrosine (IDT) contents in cell walls isolated from Wt, *prx01,44,73* triple mutant, PRX<sup>OE</sup> lines and mutant lines with under-glycosylated EXTs. P-values were determined by one-way ANOVA, (\*\*\*) P<0.001, (\*\*) P<0.01. STD=Standard Deviation. Values significantly different than Wt are highlighted in blue if higher and in light blue if lower than Wt Col-0.

	ng Tyr/ $\mu$ g CW (STD)	ng IDT/ $\mu$ g CW (STD)
Wt Col-0	7.799 $\pm$ 0.26	0.853 $\pm$ 0.08
<i>prx01,44,73</i>	9.588 $\pm$ 0.31**	0.963 $\pm$ 0.02
35S:PRX44	8.649 $\pm$ 0.07	0.953 $\pm$ 0.04
35S:PRX73	8.700 $\pm$ 0.12	1.042 $\pm$ 0.02**
<i>under O-glycosylated EXTs</i>		
<i>sergt1-1 rra3</i>	3.530 $\pm$ 0.08***	0.235 $\pm$ 0.01***
<i>p4h5 sergt1-1</i>	3.766 $\pm$ 0.06***	0.225 $\pm$ 0.02***

878  
879

880 **Table S1.** Volume and average diameter measurements of EXTs from molecular dynamics  
 881 simulations. These magnitudes were measured in the fully extended EXT system. Values shown are  
 882 the mean  $\pm$  standard deviation.  
 883

	<b>Non-glycosylated EXT</b>	<b>O-glycosylated EXT</b>	<b>O-glycosylated EXT (protein only)</b>
Volume /nm <sup>3</sup>	280 $\pm$ 30	1080 $\pm$ 50	450 $\pm$ 30
EXT length /nm	65 $\pm$ 2	70 $\pm$ 2	70 $\pm$ 2
Average diameter /nm	2.4	4.5	2.9
Distance Tyr-Tyr			
0-5 Å	20%	25%	-
5-7 Å	55%	65%	-

884

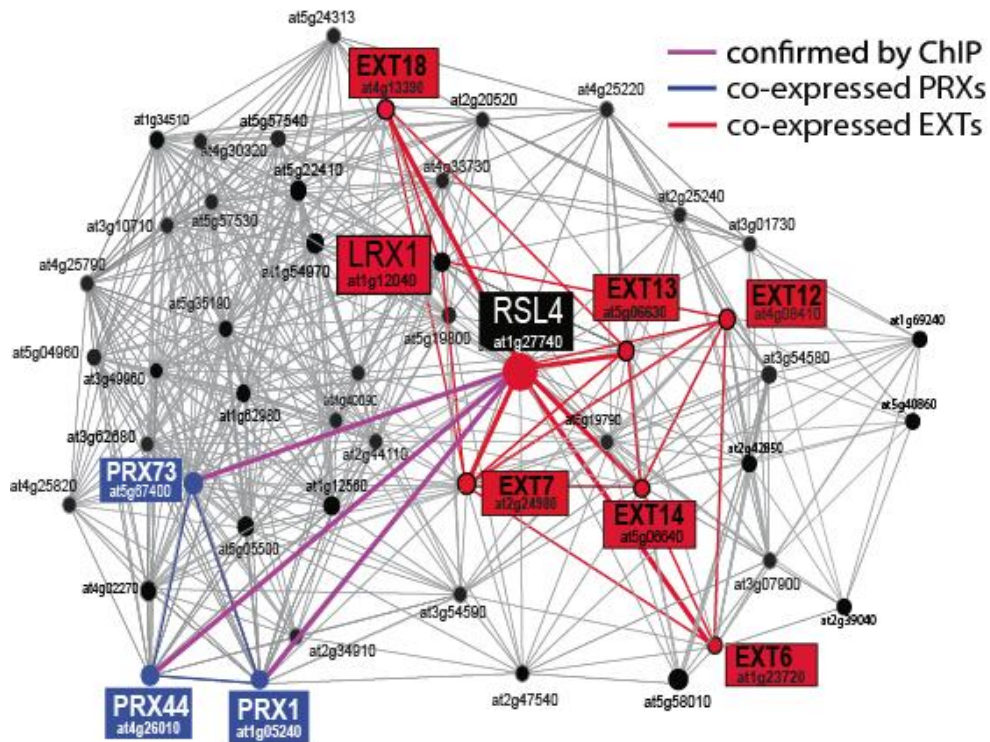
885

886 **Table S2.** Mutants and transgenic lines generated and used in this study.

887

Line name	Gene construct/ mutant lines code	References
<b>SS-TOM-Long-EXT #2</b>	35Spromoter::SS-TOMATO-longEXT	This study
<b>SS-TOM-Long-EXT #7</b>	35Spromoter::SS-TOMATO-longEXT	This study
<b>SS-TOM-Long-EXT #4</b>	35Spromoter::SS-TOMATO-longEXT/ <i>prx01,44,73</i>	This study
<b>SS-TOM-Long-EXT #6</b>	35Spromoter::SS-TOMATO-longEXT/ <i>prx01,44,73</i>	This study
<b>SS-TOM #2</b>	35Spromoter::SS-TOMATO	This study
<b>SS-TOM #5</b>	35Spromoter::SS-TOMATO	This study
<b>SS-TOM #1</b>	35Spromoter::SS-TOMATO/ <i>prx01,44,73</i>	This study
<b>SS-TOM #2</b>	35Spromoter::SS-TOMATO/ <i>prx01,44,73</i>	This study
<b>PRX01::GFP</b>	PRX01promoter::GFP/Wt Col-0	This study
<b>PRX44::GFP</b>	PRX44promoter::GFP/Wt Col-0	This study
<b>PRX73::GFP</b>	PRX73promoter::GFP/Wt Col-0	This study
<b>35S::PRX01-1</b>	35Spromoter::PRX01-GFP/Wt Col-0	This study
<b>35S::PRX01-2</b>	35Spromoter::PRX01-GFP/Wt Col-0	This study
<b>35S::PRX44-3</b>	35Spromoter::PRX44-GFP/Wt Col-0	This study
<b>35S::PRX44-4</b>	35Spromoter::PRX44-GFP/Wt Col-0	This study
<b>35S::PRX73-2</b>	35Spromoter::PRX73-GFP/Wt Col-0	This study
<b>35S::PRX73-3</b>	35Spromoter::PRX73-GFP/Wt Col-0	This study
<b>35S::PRX01-8</b>	35Spromoter::PRX01-GFP/ <i>prx01,44,73</i>	This study
<b>35S::PRX44-1</b>	35Spromoter::PRX01-GFP/ <i>prx01,44,73</i>	This study
<b>35S::PRX44-2</b>	35Spromoter::PRX44-GFP/ <i>prx01,44,73</i>	This study
<b>35S::PRX73-2</b>	35Spromoter::PRX44-GFP/ <i>prx01,44,73</i>	This study
<b>35S::PRX73-3</b>	35Spromoter::PRX73-GFP/ <i>prx01,44,73</i>	This study
<i>prx01,44,73</i>	<i>prx01-2</i> (SALK_103597) <i>prx44-2</i> (SALK_057222) <i>prx73-3</i> (SALK_009296)	This study
<i>sgt1-1 rra3</i>	<i>sgt1-1</i> (SALK_054682) <i>rra3</i> (GABI_233B05)	Velasquez et al. 2015a

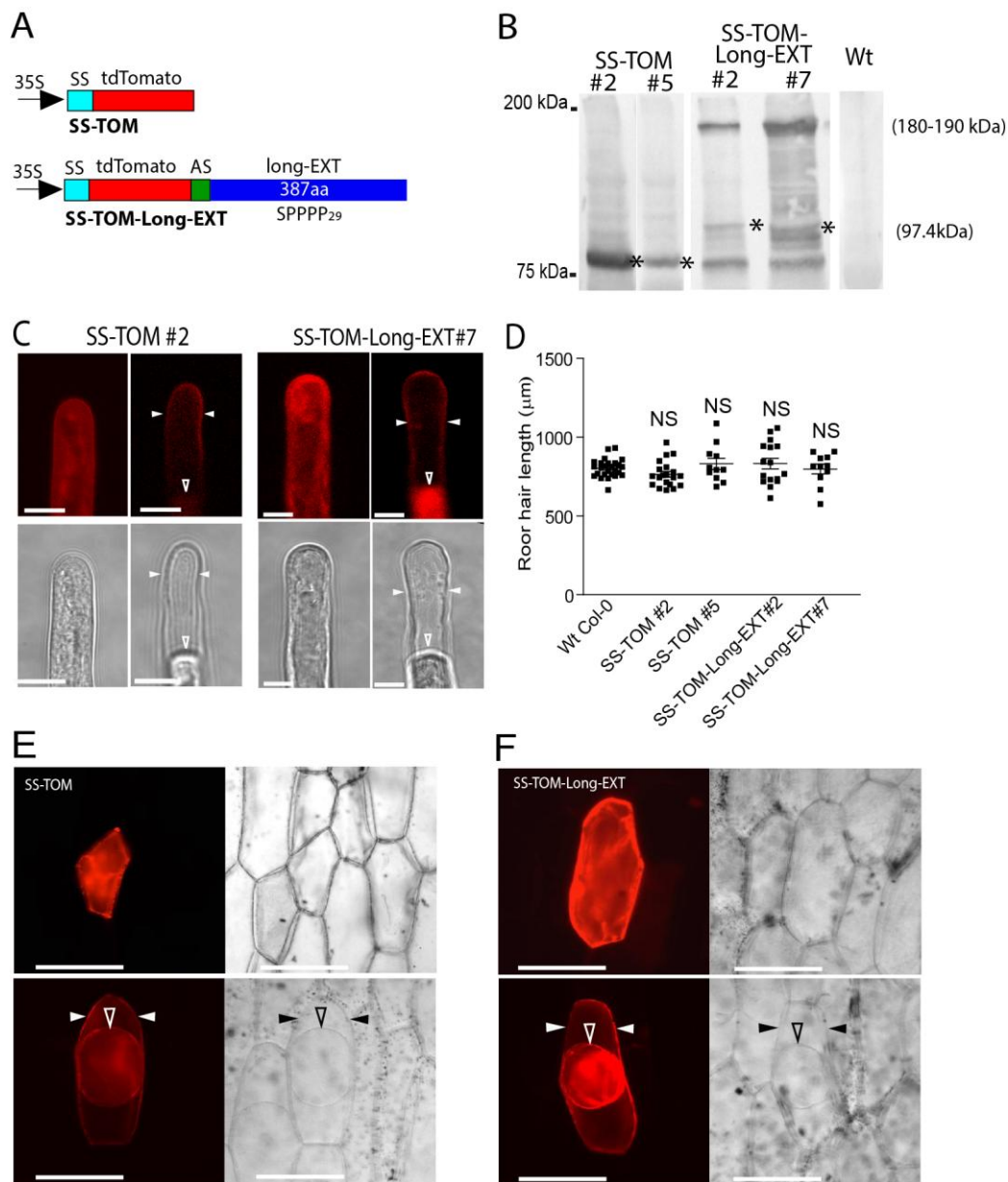
888



889

890

891 **Figure S1. Root hair transcriptional co-expression network.** PRXs, EXTs, and the transcriptional  
 892 regulator RSL4 are highlighted. RSL4 was used as gene bait to narrow down the number of co-  
 893 expressed genes. Transcriptional connections between RSL4 (in black), EXTs (in red) and PRXs genes  
 894 (in blue). The co-expression network was identified from PLaNet ([http://aranet.mpimp-  
 895 golm.mpg.de/aranet](http://aranet.mpimp-golm.mpg.de/aranet)) (Mutwil et al., 2011) and trimmed to facilitate readability. Chromatin  
 896 immunoprecipitation assay (ChIP) showed that RSL4 binds and controls the expression of  
 897 PRX01,44,73 (Mangano et al. 2017). Figure modified from Marzol et al. (2018).



899

900

901 **Figure S2. EXT reporter is targeted to root hair and onion epidermal cell walls.**

902 (A) Schematic diagrams of SS-TOM and SS-TOM-Long-EXT constructs expressed under the control of  
 903 the 35S promoter in *Arabidopsis* plants. SS, tomato polygalacturonase signal sequence. AS, Ala-  
 904 spacer, 6 alanines between tdTomato (TOM) and Long-EXT domain. Long-EXT, C-terminal 405 amino  
 905 acids of *SIPEX1*, which includes only two tyrosines at the C-terminus.

906 (B) Expression and detection of EXT-reporters in homozygous *Arabidopsis* lines. Lines expressing  
 907 detectable levels of SS-TOM (lines #2 and #5) and SS-TOM-Long-EXT (lines #2 and #7) showed  
 908 similarly unexpectedly large sizes of protein on the Western blot, with bands much larger than the

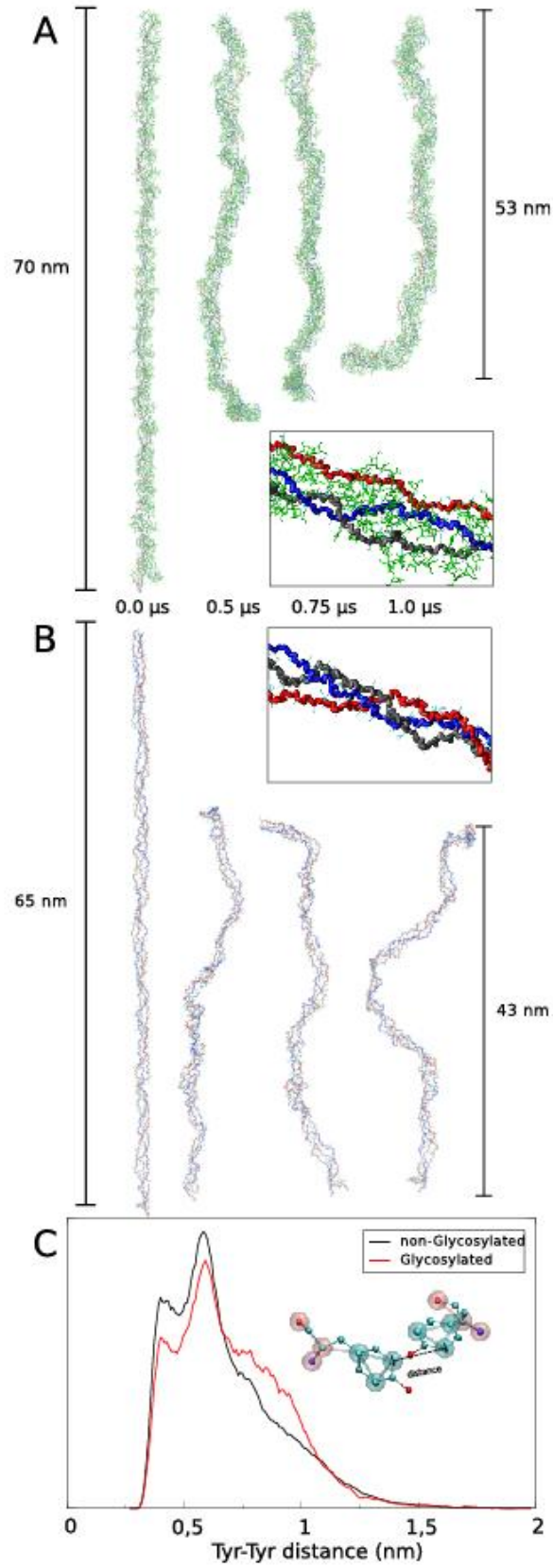
909 predicted size of the unmodified TOM tagged Long-EXT protein. The predicted molecular size for SS-  
910 TOM protein is around 54.2 kDa and for SS-TOM-Long-EXT is around 97.4 kDa are indicated with  
911 asterisks (\*). All the gel blots shown are part of the same run.

912 (C) Expression of SS-TOM and SS-TOM-Long-EXT reporters in *Arabidopsis* root hair cells. (Top)  
913 Fluorescence images showing cell-wall localization of the reporter protein: left, cells with normal  
914 cytoplasm; right, cells after plasmolysis in 1 M NaCl. (Bottom) Bright-field images of the same cells  
915 shown above. Cell wall location is denoted with solid arrowheads while plasma membrane is  
916 indicated with an unfilled arrowhead. Scale bar = 10  $\mu$ m.

917 (D) Root hair phenotype of Wt, SS-TOM (#2 and #5) and SS-TOM-Long-EXT (#2 and #7) (in Wt  
918 background) as box-plot. Horizontal lines show the means. NS = not significantly different,  
919 determined by one-way ANOVA.

920 (E) Onion epidermis expressing SS-TOM. (On the right) Bright field images. (On the bottom) cells  
921 were plasmolyzed in 1 M NaCl. Cell wall location is denoted with solid arrowheads while plasma  
922 membrane is indicated with an unfilled arrowhead. Scale bar = 100  $\mu$ m. SS = Signal Peptide. TOM =  
923 Tomato fluorescent protein.

924 (F) Onion epidermis expressing SS-TOM-Long-EXT. (On the right) Bright fields images. (On the  
925 bottom) Cells were plasmolyzed in 1 M NaCl. Cell wall location is denoted with solid arrowheads  
926 while plasma membrane is indicated with an unfilled arrowhead. Scale bar = 100  $\mu$ m. SS = Signal  
927 Peptide. TOM = Tomato fluorescent protein. Long-EXT = C-terminal 290 amino acids of *Solanum*  
928 *lycopersicum* (SI) *SIPeX1*.

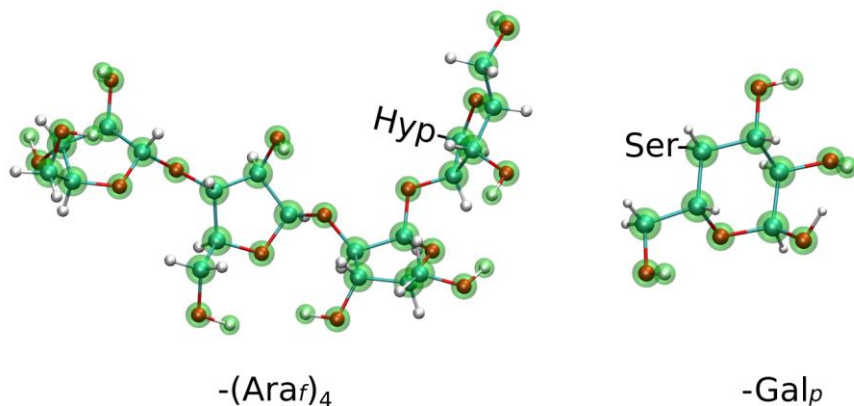


930 **Figure S3. Effect of the *O*-glycosylation status on the triple helix EXT assembly and Tyr-Tyr**  
931 **distances.**

932 Selected snapshots of the *O*-glycosylated (**A**) and non-glycosylated (**B**) triple EXT chain molecular  
933 dynamics (MD) trajectory, showing the stability of the triple helix during a 1  $\mu$ s MD simulation. The  
934 results obtained in these simulations highlight the importance of the triple-helix EXT in overall  
935 protein stability, and especially the maintenance of the fibril-like structure. Peptide chains are  
936 depicted in red, black and blue and glycans in green. In these simulations the peptide chains are  
937 allowed to move freely inside the simulation box, without any restrictions. Insets: a snapshot of a 25  
938 amino acid portion of the triple helix taken from the CG MD trajectory.

939 (**C**) Distribution of the Tyr-Tyr distances along the MD simulations for the glycosylated (red line) and  
940 non-glycosylated (black line) states. Distances are measured between the *C-orthos* of each Tyr  
941 residue (as depicted in the inset of the figure).

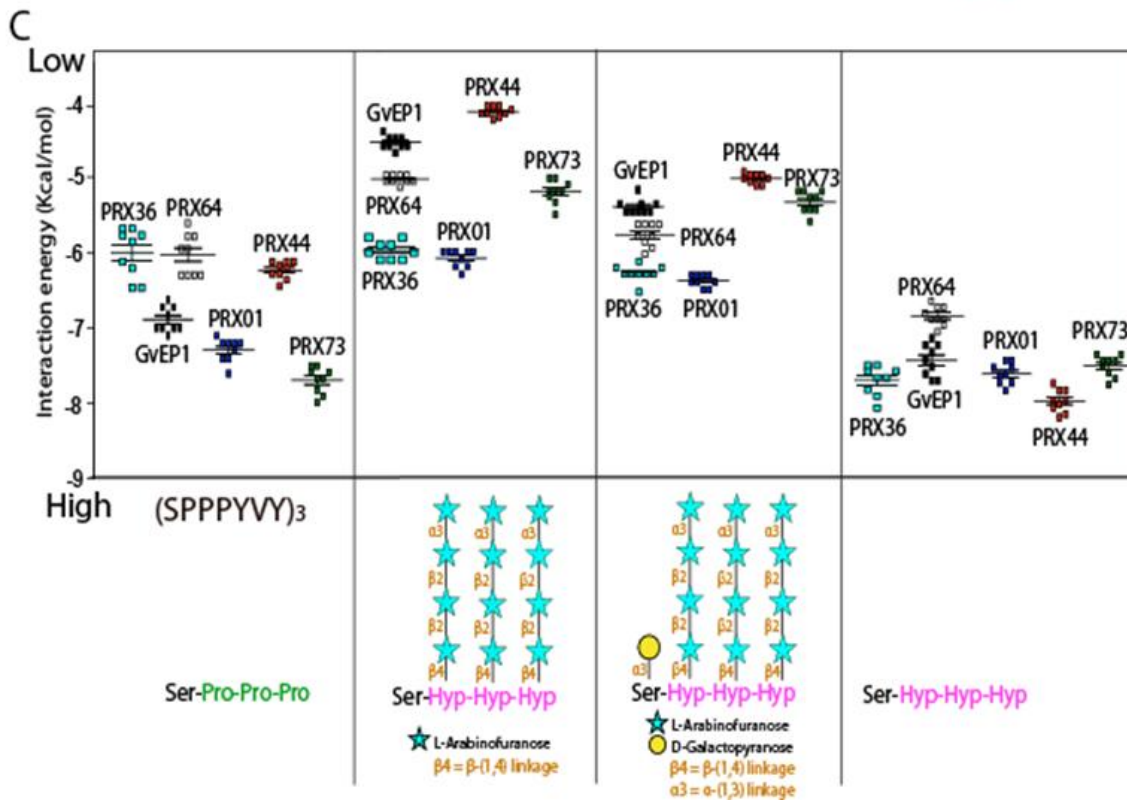
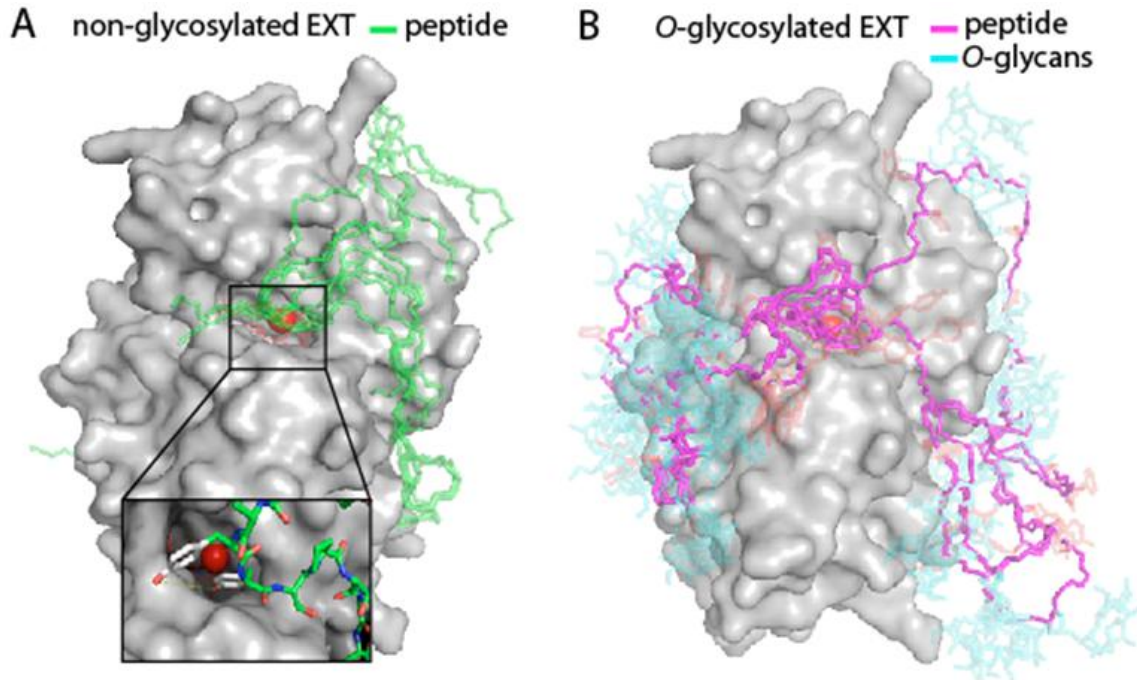
942



943

944

945 **Figure S4. Coarse-grained models for tetra-arabinofuranose and galactopyranose moieties (diffuse**  
946 **green spheres) superimposed on all atom description (solid spheres connected by tubes).**  
947 Interaction points or beads are located in the position of the heavy atoms and hydrogens  
948 corresponding to hydroxyl groups. The latter were included due to the importance of directional  
949 hydrogen bond-like interactions in this class of molecules. Mass and Lennard-Jones parameters of  
950 CG beads and spring constants for intramolecular interactions were chosen to be compatible with  
951 the SIRAH coarse-grained model (parameters are available upon request).



953

954

955 **Figure S5. Interaction by an *in silico* docking approach of PRX01, PRX44 and PRX73 with EXT**  
 956 **peptides.**

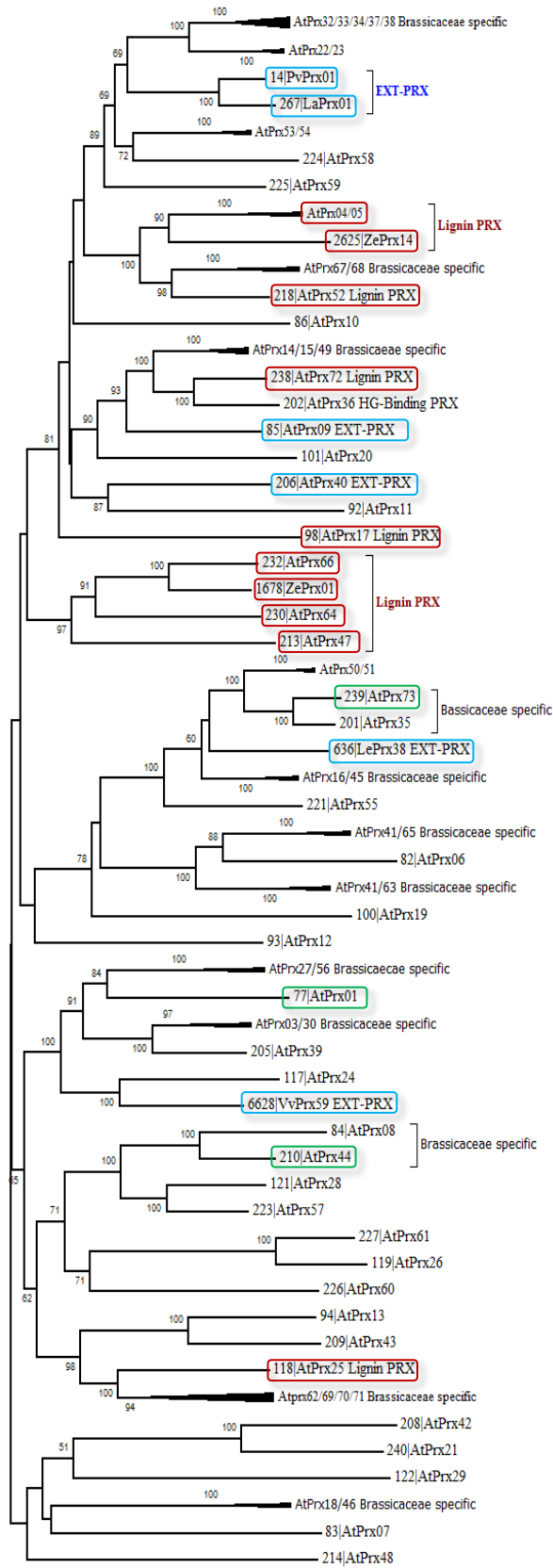
957 **(A,B)** Ten docking results for each EXT *O*-glycosylation state are shown superimposed on the PRX44  
958 protein surface to evaluate the consistence of docking sites.

959 **(A)** Model of PRX44 (protein surface shown in gray) complexed to a non-*O*-glycosylated EXT  
960 substrate (SPPPYVY)<sub>3</sub> (in green, depicted as sticks). Heme is depicted as thin sticks while iron is a red  
961 sphere. Bottom inset, two close tyrosine residues dock near to the possible active site of PRX44.

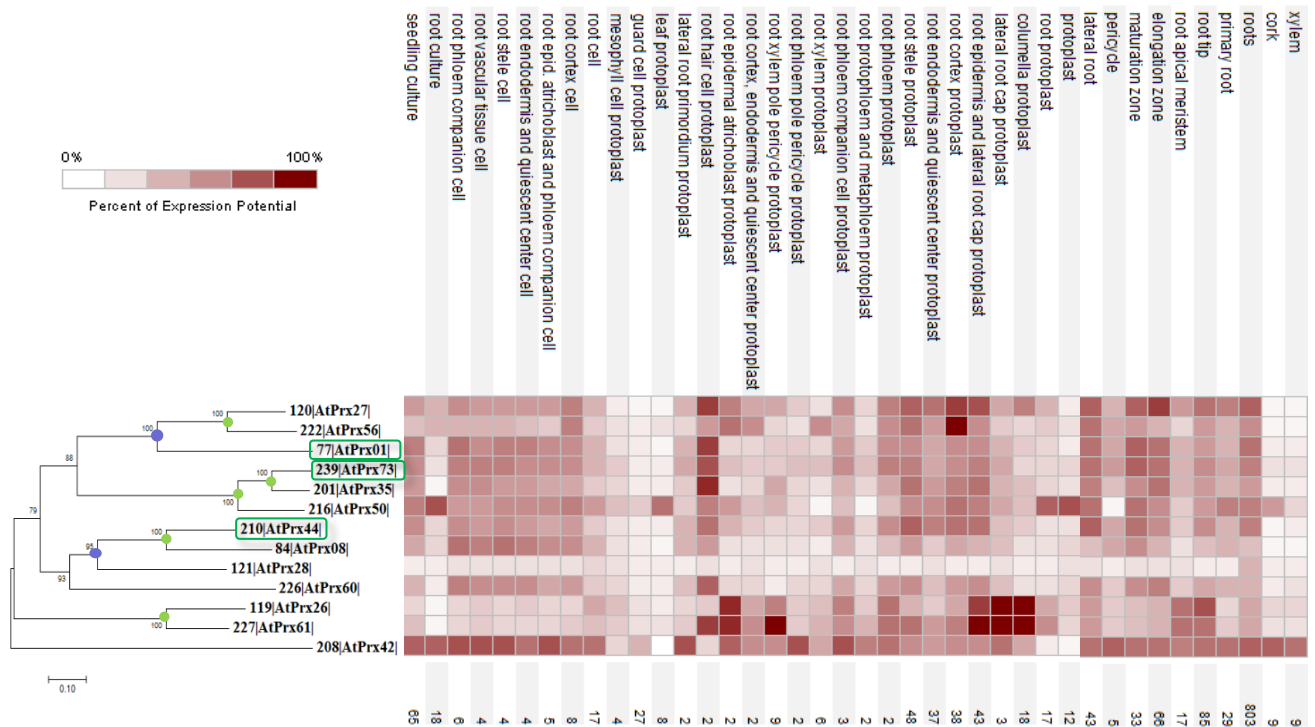
962 **(B)** Model of PRX44 (protein surface shown in gray) complexed to an *O*-glycosylated-EXT substrate  
963 (protein backbone shown in magenta, and *O*-glycans shown in light blue, both depicted as sticks).  
964 Heme is depicted as thin sticks while iron is a red sphere. Arabino-galactosylated EXT peptide =  
965 [(S000YVY)<sub>3</sub>-AG].

966 **(C)** Comparison of the binding energy of different peroxidases to EXT substrates with different degrees of *O*-  
967 glycosylation. A non-hydroxylated EXT peptide (SPPPYVY)<sub>3</sub>, a hydroxylated but not *O*-glycosylated EXT peptide  
968 [(S000YVY)<sub>3</sub>; O=hydroxyproline], only arabinosylated EXT-peptide [(S000YVY)<sub>3</sub>-A], and arabino-  
969 galactosylated EXT peptide [(S000YVY)<sub>3</sub>-AG] were analyzed.



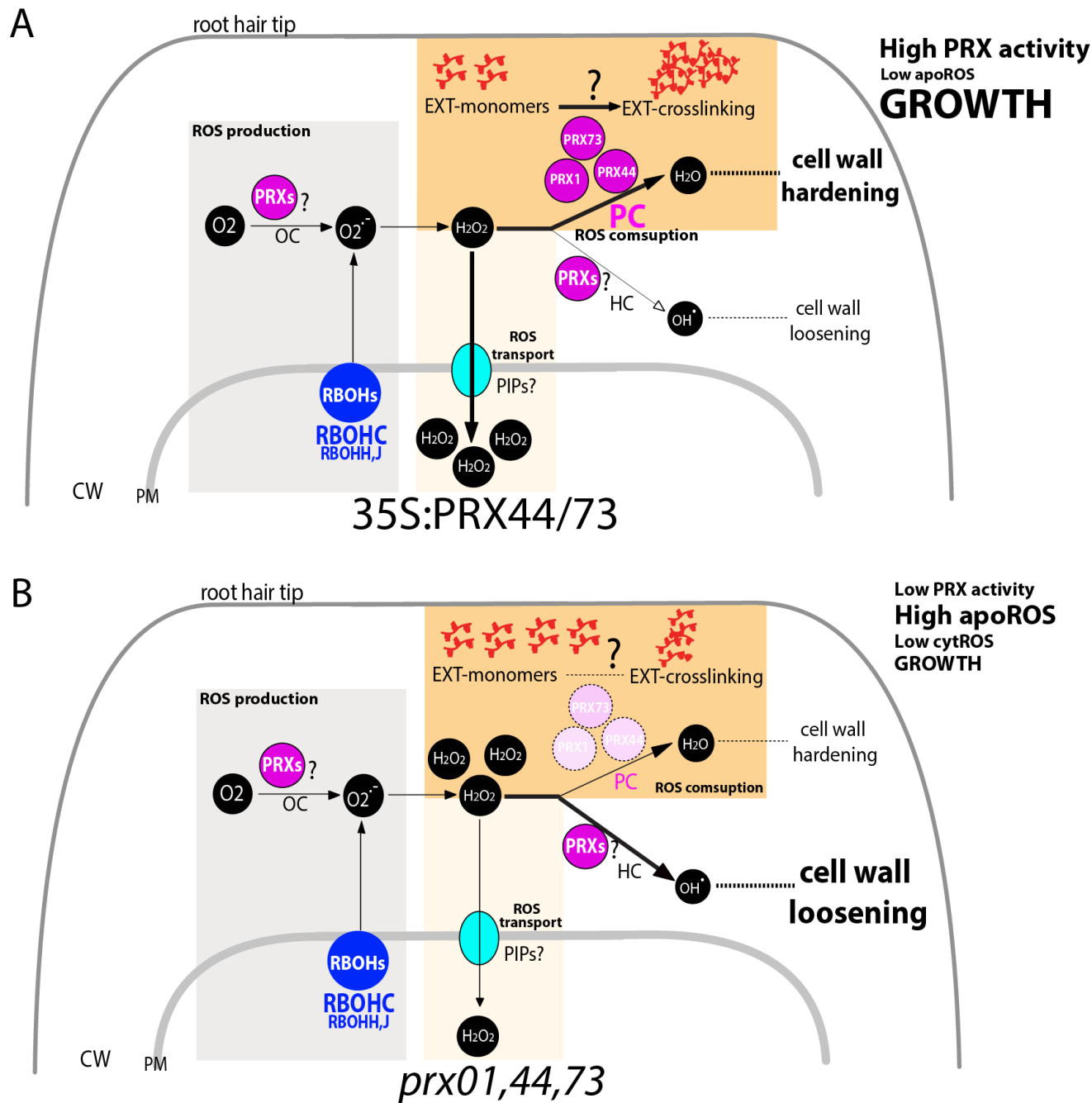


972 **Figure S6. Evolutionary relationships of CIII Prx with putative extensin cross-linking activity.**  
973 The 73 Class-III Peroxidase protein sequences from *A. thaliana*, two putative Lignin PRX from *Zinnia*  
974 *elegans* and four putative EXT-PRX from *Lupinus album*, *Solanum lycopersicum*, *Phaseolus vulgaris*  
975 and *Vitis vinifera*, have been aligned with ClustalW and the tree constructed using the Neighbor-  
976 Joining method (Saitou and Nei, 1987). The analyses were conducted in MEGA7 (Kumar, 2016). Class-  
977 III PRXs with putative EXT-PRX activity or Lignin PRX activity were surrounded in blue and red  
978 respectively. The three Class-III PRXs studied in the present work were surrounded in green.  
979 Branches of the tree with sequences resulting from duplication events only detected in Brassicaceae  
980 have collapsed to simplify the tree topology.



983 **Figure S7. Evolutionary and root tissue expression relationships of putative EXT-PRXs in**  
 984 **Arabidopsis.**

985 The evolutionary history of Class III PRXs in root hair associated has been conducted with 15 CIII PRX  
 986 protein sequences of *A. thaliana*. They have been aligned with ClustalW and the tree constructed  
 987 using the Neighbor-Joining method (Saitou and Nei, 1987). The analyses were conducted in MEGA7  
 988 (Kumar, 2016). The sequences of AtPRX01/02 and AtPRX50/51 are either identical or very close,  
 989 leading to only two independent expression profiles from Affymetrix data. A brown (max value)-to-  
 990 cream (min value) heatmap was drawn from 105 anatomical parts from data selection available from  
 991 AT\_AFFY\_ATH1-0 and plotted in front of each branch and using Genevestigator. The 3 CIII PRX  
 992 studied in the present work were surrounded in green. Green and blue circles correspond to  
 993 duplication posterior to Brassicaceae and to Dicotyledons emergences respectively. All protein  
 994 sequences are available using their ID number (<http://peroxibase.toulouse.inra.fr>, (Savelli et al.,  
 995 2019). Numbers indicate the amount of dataset available for each tissue.



997

998

999 **Figure S8. Current model of PRX01, PRX44, and PRX73 function linking ROS homeostasis and EXT**  
 1000 **crosslinking in the root hair cell walls.** ROS homeostasis in the apoplast includes ROS production,  
 1001 ROS consumption, and ROS transport to the cytoplasm. ROS as superoxide ion ( $O_2^{\cdot-}$ ) is primarily  
 1002 produced by RBOHC and by RBOHH,J [based on Mangano et al. (2017)] and, possibly, by unknown  
 1003 PRXs in the root hair tip, and then dismutated to hydrogen peroxide ( $H_2O_2$ ). **(A)** It is proposed that  
 1004 high levels of PRX44 or PRX73 during the peroxidative cycle (PC) (as found in 35S:PRX44-GFP and

1005 35S:PRX73-GFP lines) might trigger a high consumption of apoplastic H<sub>2</sub>O<sub>2</sub> (low <sub>apo</sub>ROS) with a  
1006 concomitant cell wall hardening. **(B)** Under low levels of all three PRXs (as found in the triple mutant  
1007 *prx01,44,73*), most of the H<sub>2</sub>O<sub>2</sub> produced accumulates in the apoplast (high <sub>apo</sub>ROS) triggering a  
1008 cessation of cell expansion. A portion of apoplastic H<sub>2</sub>O<sub>2</sub> might be transported into the cytoplasm by  
1009 aquaporins (PIPs). The balance between cell wall hardening and cell wall loosening processes might  
1010 be compromised, affecting polar root hair growth. CW = cell wall; PM = plasma membrane; HC =  
1011 hydroxylic cycle; OC = oxidative cycle. PIP= Plasma membrane Intrinsic Proteins (aquaporins).

1012  
1013  
1014  
1015  
1016  
1017  
1018  
1019  
1020  
1021  
1022  
1023  
1024  
1025  
1026  
1027  
1028  
1029  
1030  
1031

**SUPPLEMENTARY REFERENCES**

Kumar, S., Stecher G., Tamura K. (2016) MEGA7: molecular evolutionary genetic analysis version 7.0 for bigger datasets. *Mol. Biol. Evol.* 33(7): 1870-1874.

Mangano S. *et al.* (2017). The molecular link between auxin and ROS-controlled root hair growth. *Proc. Natl. Acad. Sci. U.S.A.* 114(20):5289-5294.

Marzol E, Borassi C, Bringas M, Sede A, Rodríguez Garcia DR, Capece L, Estevez JM. (2018). Filling the Gaps to Solve the Extensin Puzzle. *Mol Plant.* 11(5):645-658.

Mutwil, M., Klie, S., Tohge, T., Giorgi, F.M., Wilkins, O., Campbell, M.M., Fernie, A.R., Usadel, B., Nikoloski, Z. and Persson, S. (2011). PlaNet: combined sequence and expression comparisons across plant networks derived from seven species. *Plant Cell*, 23, 895– 910.

Saitou N, Nei M. (1987). The neighbor-joining method: a new method for reconstruction of phylogenetic trees. *Mol Biol Evol*4:406–25.

Savelli B., Li Q., Webber M., Jemmat A.M., Robitaille A., Zamocky M., Mathe C., Dunand C. (2019). RedoxiBase a database for ROS homeostasis regulated proteins. *Redox Biol.* doi.org/10.1016/j.redox.2019.101247.

Velasquez SM, Marzol E, Borassi C, Pol-Fachin L, Ricardi MM, Mangano S, Denita JS, Salgado SJ, Gloazzo DJ, Marcus SE. (2015a). Low sugar is not always good: Impact of specific O-glycan defects on tip growth in Arabidopsis. *Plant Physiology* 168, 808–813.